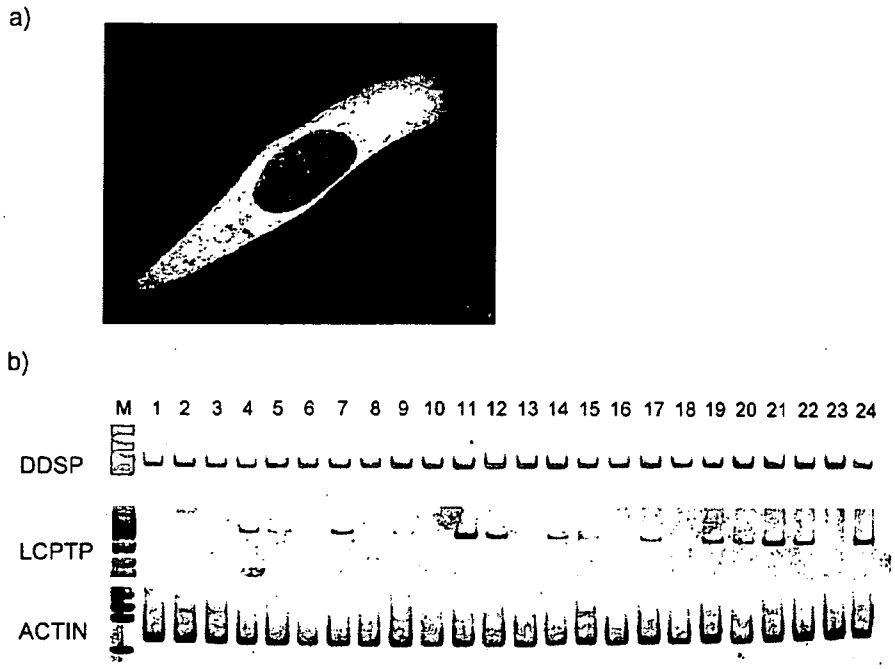

Fig. 3. Subcellular and tissue distribution of DDSP. (a) Cytoplasmic localization of DDSP. The DDSP cDNA sequence was ligated in-frame into pEGFP, transfected into COS7 cells and then subjected to a confocal microscopic analysis. (b) Tissue distribution of DDSP and LCPTP/HePTP. The 2 sequence specific sets of primers for DDSP (top panel) or LCPTP/HePTP (middle panel) were used for RT-PCR. The bottom panel represents the RT-PCR amplifying β-actin mRNA. Lanes are 1: brain; 2: heart; 3: kidney; 4: spleen; 5: liver; 6: colon; 7: lung; 8: small intestine; 9: skeletal muscle; 10: stomach; 11: testis; 12: placenta; 13: salivary gland; 14: thyroid; 15: adrenal; 16: pancreas; 17: ovary; 18: uterus; 19: prostate; 20: skin; 21: lymphocyte; 22: bone marrow; 23: fetal brain; 24: fetal liver.

fected cells with DHEA or treatment of the transfected PEER with or without PMA and A23187 did not significantly change the homogeneous cytoplasmic distribution of GFP-fluorescence (data not shown). Taken together with the observations of the DSP activities, these results indicated that 1–20 encoded a novel member of the cytoplasmic DSP family. We tentatively named this novel DSP DHEA-enhanced DSP (DDSP).

3.4. Profiles of tissue distribution, PMA/A23187 induction and hormonal regulation of DDSP mRNA

To discriminate the mRNA expression of DDSP (full-length 1–20) as potentially DSP from those of tissue-specific LCPTP/HePTP, we designed 2 sets of primers for RT-PCR experiments: one to amplify the sequence specific to DDSP and another specific to LCPTP/HePTP (Fig. 1b). Using these 2 sets of primers, we investigated the tissue distribution and the response to PMA/A23187 or hormonal stimulation. In strong contrast to the restricted tissue distribution of LCPTP/HePTP mRNA preferentially expressed in hematopoietic tissues (and in testis at RT-PCR level), the basal expression of DDSP mRNA was observed by RT-PCR at a similar expression level in all types of human tissues examined (Fig. 3b).

In PEER cells without PMA/A23187 stimulation, the basal expression level (standardized by the fragment length and β-actin expression) of DDSP mRNA was about 20 to 30% of that of LCPTP/HePTP. PMA/A23187 treatment rapidly increased the DDSP mRNA expression within 1 h and then reached a maximum level (5- to 7-fold) at 3 h poststimulation. 100 nM DHEA further increased the DDSP mRNA level by 2.5- to 3-fold at 3 h poststimulation (Fig. 4a). On the other hand, LCPTP/HePTP-specific RT-PCR showed a constitutive expression even in the untreated PEER cells, and PMA/A23187 stimulation with or without DHEA did not significantly alter the expression (Fig. 4b). Costimulation with either 100 nM dexamethasone (DEX), 1 μM DHEA sulfate (DHEAS) or 10 nM dihydrotestosterone (DHT) did not exert the reproducible induction of DDSP mRNA level in the repeated experiments, while the 10 nM 17β-estradiol (E2) treatment sometimes slightly repressed the PMA/A23187-induced DDSP expression. These steroid hormones, including DHEA, did not affect the mRNA levels of LCPTP/HePTP. In Fig. 4c and d, representative results of RT-PCR experiments were shown.

3.5. Interaction of DDSP with the MAPK cascade

To observe the interactions of DDSP with MAPK, we transfected a plasmid expressing a flag-DDSP fusion product into NIH3T3 mouse fibroblasts and then tested the binding of DDSP with activated endogenous ERK1/2, p38-MAPK or JNK by immunocoprecipitation. Western blotting showed that DDSP specifically bound to phosphorylated p38-MAPK activated by hyperosmotic 0.5M NaCl stimulation, but not to

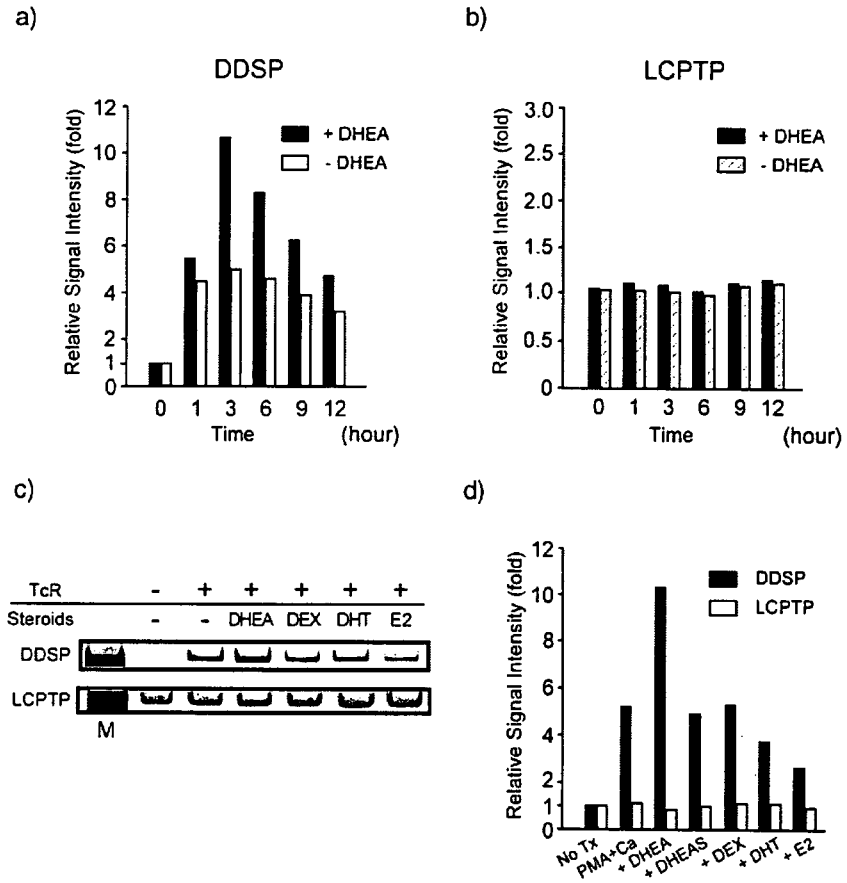

Fig. 4. The differential profiles of mRNA induction between DDSP and LCPTP/HePTP. The same primer set used in Fig. 3b was used for the RT-PCR. (a) The effect of a physiological concentration (100 nM) of DHEA on the expression of DDSP in TcR-activated PEER cells. PEER cells were stimulated by PMA and calcium ionophore A23187 with (filled bar) or without (open bar) DHEA. The relative induction values compared with the basal mRNA expression with no PMA/A23187 treatment, standardized by β-actin expression, are expressed as the-fold induction. (b) Effect of 100 nM DHEA on the expression of LCPTP/HePTP in TcR-activated PEER cells. PEER cells were stimulated as described above. The relative induction values are expressed as in Panel (a): Filled bars: with DHEA; hatched bars: without DHEA. (c) Effects of various steroid hormones on the mRNA expression of DDSP or LCPTP/HePTP. Representative results of the RT-PCR experiments are shown. The PEER cells were treated with PMA and calcium ionophore A23187 in the absence of any steroid hormones, or in the presence of 100 nM DHEA (DHEA), 100 nM dexamethasone (DEX), 10 nM dihydrotestosterone (DHT), or 1 nM 17β-estradiol (E2). The RNAs were extracted after 3 h of treatment and then subjected to semiquantitative RT-PCR using a set of primers specific for DDSP (upper panel) or LCPTP/HePTP (lower panel). (d) Schematic representation of the effects of the various steroid hormones. In this experiment, treatment with 1 μM of DHEA-sulfate (DHEAS) was included. The relative induction of each sequence in the PEER cells compared with the basal mRNA expression with no treatment (No Tx) is expressed as the-fold induction. The PEER cells were treated with PMA and calcium ionophore A23187 in the absence of any steroid hormones (PMA+Ca) or in the presence of 100 nM DHEA (DHEA), 1 μM DHEAS (DHEAS), 100 nM dexamethasone (DEX), 10 nM dihydrotestosterone (DHT) or 1 nM 17β-estradiol (E2), respectively. Filled bars: DDSP mRNA; open bars: LCPTP/HePTP mRNA.

activated ERK1/2 or JNK (Fig. 5a and b). This finding also suggested that the N-terminal 13 aa residues of DDSP (corresponding to aa residues 49–61 of LCPTP) were required for and enough for P38-MAPK-binding.

The inactivation of the phosphorylated p38-MAPK by DDSP was shown by the dephosphorylation of the phosphorylated p38-MAPK. DDSP specifically dephosphorylated the endogenous p38-MAPK, activated by hyperosmotic stimulation using 0.5 M NaCl, in NIH3T3 cells that were transiently transfected with plasmids expressing flag-tagged DDSP, while the phosphorylated ERK or JNK were not dephosphorylated (Fig. 6a). The p38-MAPK-specific inactivation was further confirmed using the pMACS system that can select transfected cells from untransfected cells and can thus enrich the transfected cells to nearly 80% after passage through an affinity column. The expression of the DDSP protein dephosphorylated the endogenous p38-MAPK activated by 0.4 M sorbitol hyperosmotic treatment, but not ERK activated by PMA treatment, in the cells selected after the enrichment (Fig. 6b). Taken together, these results indicated that DDSP inactivates the MAPK cascade in a p38-MAPK-specific fashion.

4. Discussion

To clarify the action of DHEA on a molecular basis, a comparison of the cellular phenotypes between the DHEA-

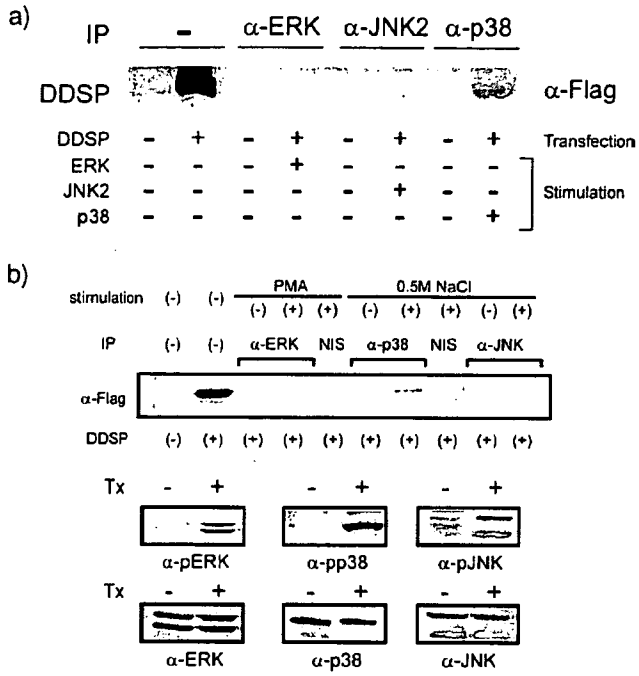

Fig. 5. Immunocoprecipitation of DDSP with ERK, p38 or JNK. (a) NIH3T3 cells transfected with a plasmid expressing flag-tagged DDSP were treated with 0.5 M NaCl for 20 min (for p38 and JNK) or with 50 ng/ml of PMA for 15 min after incubation in a serum free medium for 15 h (for ERK). The endogenous ERK, p-38 or JNK in the whole cell lysates from the treated cells was immunoprecipitated with an anti-ERK, -p38 or -JNK antibody, respectively, and then Western blotting was performed using an anti-flag antibody. DDSP specifically interacts with the endogenous phosphorylated p38-MAPK. (b) Immunoprecipitation and Western blot were performed as in Panel (a) (top panel). NIS: non-immune serum. In the middle and bottom panels, the three pairs of whole cell lysates used for the immunoprecipitations in the top panel were probed to confirm the activation of each MAPK, using antibodies against phosphorylated MAPKs (middle panels: anti-pERK, anti-pp38, anti-pJNK) or total MAPKs (bottom panels: anti-ERK, anti-p38, anti-JNK). Tx: PMA-treatment for the activation of ERK or 0.5 M NaCl treatment for the activation of p38- or JNK-MAPK.

treated and untreated cells led to the isolation of the p38 MAPK phosphatase, DDSP. We demonstrated that this novel member of the PTPN7 locus-derived family was a candidate for one of the target genes of DHEA. One explanation for the biological action of DHEA is that DHEA exerts its functions after being biotransformed into biologically more active androgens and estrogens in either the peripheral tissues or the target cells (intracrine mechanism) [23]. In contrast, the superinduction effect of DHEA on the DDSP mRNA level was specific according to the results shown in Fig. 4. As one of the broad range of actions caused by DHEA, DHEA(-S) has been used for some collagen disease as adjunctive treatment expecting the immune modulating action [24–27] (for review). In this regard, the lymphocytes from the periphery of systemic lupus erythematosus (SLE) patients had a more activated p38 MAPK, as well as ERK or JNK, status immediately ex vivo when compared with lymphocytes from the periphery of normal individuals [28].

We propose a mechanism to explain, at least in part, this immune modulating action, namely that DHEA exerts the anti-inflammatory action by directly suppressing the p38-MAPK cascade. Recently, p38-MAPK has received much attention as a potential drug target for diseases such as rheumatoid arthritis, endotoxic shock, inflammatory bowel disease, osteoporosis and many others [29]. Our findings suggest that DHEA augments the negative feedback regulation of MAPK cascades that have become overactivated due to stress or cytokine signals via a specific set of MAPK phosphatases in many human tissues. In the vascular smooth muscle cell, p38-MAPK activation by PDGF is inhibited by low molecular weight PTPs, thus suggesting that MAPK phosphatases are important negative regulators for the vascular smooth muscle cell growth and migration processes leading to the progression of atherosclerosis [8,9,30]. Apart from the action on the MAPK cascade, it has been demonstrated that DHEA inhibits the nuclear translocation of nuclear factor-κB (NF-κB) probably due to the induction of peroxisome via the peroxisome proliferator activated receptor α (PPARα) [31], or that DHEA inhibits the binding of transcription factor activator protein-1 (AP-1) to DNA [32], thus exerting the anti-inflammatory action. To date, no receptor for DHEA or DHEAS has yet been cloned. The presence of cytoplasmic DHEA binding activity has been demonstrated in human peripheral blood monocytes [7], vascular smooth muscle cell [9] and human T lymphocytes [16], although according to the human genome project, it seems unlikely that a classical steroid hormone receptor-type DHEA receptor exists. Interestingly, Liu et al. reported the existence of the putative membrane receptor for DHEA [33]. DHEA may directly exert its

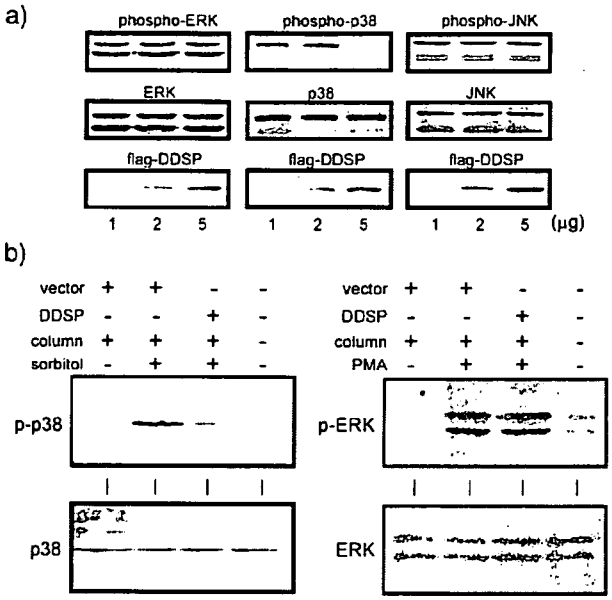

Fig. 6. DDSP dephosphorylates p38-MAPK. (a) Phosphatase activities of DDSP on ERK, p38 or JNK. NIH3T3 cells were transfected with 1, 2 or 5 μg of a plasmid expressing flag-tagged DDSP (left lane, middle lane and right lane, respectively, in each panel). The total amounts of the transfected plasmids were kept constant by adding the empty vector plasmid. The transfected cells were treated as in Fig. 5, and then the whole cell lysates were subjected to Western blotting. The antibodies were raised against phosphorylated (phospho-) MAPKs (top panels), total MAPKs (middle panels) or flag (bottom panels). (b) pMACS experiment showing the p38-MAPK-specific dephosphorylation. NIH3T3 cells were transfected in 10 cm dishes with 20 μg of pMACS-DDSP (DDSP), or pMACSKkII vector (vector) as a control. The transfected cells were enriched after column separation and then treated with 0.4 M sorbitol for 20 min to activate p38-MAPK or with 50 ng/ml PMA to activate ERK. Western blotting was performed using an antibody against phosphorylated p38-MAPK (upper left) or ERK (upper right) (shown as p-p38 and p-ERK, respectively) or total p38-MAPK (lower left) or ERK (lower right) (shown as p38 and ERK, respectively). In this experiment, the column passage alone mildly activated p38-MAPK and caused the basal level phosphorylation of p38-MAPK. The expression of DDSP specifically inactivated the p38-MAPK to the basal level.

action not through the nuclear receptor but through the signal transduction system, such as MAPK system, activated by membrane-type receptors.

The MAPK cascade is regulated by both the phosphorylation and dephosphorylation of the members of the cascade. LCPTP/HePTP has been shown to act as a phosphotyrosine-specific phosphatase for both ERK (ERK2) and p38-MAPK [34,35], and one report showed HePTP as the ERK2-specific phosphatase in the myelogenous leukemia cell line K562 [36]. While LCPTP/HePTP does not dephosphorylate phosphoserine/phosphothreonine residues in ERK1/2 [34], recent findings have revealed that a subfamily of PTP dephosphorylate not only the phosphotyrosine but also the phosphoserine/phosphothreonine residue, and was thus called DSP [37]. When we tested whether or not the DDSP protein possesses phosphatase activities for the phosphoserine/phosphothreonine residue, the DDSP protein also caused a rapid loss of the phosphate from the phosphothreonine as well as from the phosphotyrosine. These results indicated that the DDSP might play a role as a DSP in vivo.

Each DSP or PTP has a restricted subcellular localization [37] (for review), while LCPTP/HePTP has been shown to localize in the cytoplasm (cytoplasmic PTP) as well [38]. DDSP was cytoplasmic as well as LCPTP/HePTP. In contrast, the mRNA profiles of the tissue distribution and the response to MAPK cascade stimulation and steroid hormone treatment were different between DDSP and LCPTP/HePTP, while DDSP was highly homologous to LCPTP/HePTP. Although the mRNA expression of LCPTP/HePTP has previously been shown to be inducible, the RT-PCR experiments using specific sets of primers suggested that the expression of LCPTP/HePTP was constitutive while the actual inducible sequence could be that of DDSP. While mRNA levels in mouse lymphocytes, detected by Northern blots, increased upon stimulation with phytohemagglutinin, lipopolysaccharide, concanavalin A, or anti-CD3 [20], the HePTP protein was present even in resting cells, and its amount increased slightly [34]. The differential mRNA expression between DDSP and LCPTP/HePTP might be due to, though not to be tested yet, the differential promoter usage.

In addition, at the protein level, the substrate specificity was different between DDSP and LCPTP/HePTP. LCPTP/HePTP binds to both ERKs and p38-MAPK through a kinase-interaction motif (KIM) located at the N-terminus of the protein and inactivates them by dephosphorylating the critical phosphotyrosine residue in their activation loop, thus playing a negative role in the TcR signaling pathway [39]. Furthermore, the binding of HePTP to ERK or p38-MAPK is in a phosphorylation-independent fashion [34]. HePTP has previously been shown to interact with both ERK1/2 and p38-MAPK via the 40 aa of the N-terminus sequence [34]. The aa residues 1 to 40 of HePTP corresponded to aa residues 22 to 61 of LCPTP (Fig. 1b). In particular, Arg41 and Arg42 play a crucial role in ERK binding [35]. DDSP lacked the first 48 aa stretch (including Arg41 and Arg42) of LCPTP required for ERK1/2 binding, while the following aa sequence was highly conserved, except for 1 aa residue (Val 220, bold line in Fig. 1b) in addition to the unique 11 aa stretch at the C' -terminus end (Fig. 1a). This may contribute to why DDSP specifically bound to and inactivated phosphorylated p38-MAPK. To date, only one molecule, Wip1, which is induced in response to ionizing radiation in a p53-dependent manner, has been shown to be a p38-specific MAPK phosphatase [40,41]. Our present study suggested the complexity of the gene regulation in the PTPN7 locus. By the mechanisms of alternative splicing and possible differential promoter usage, PTPN7 may encode at least 3 protein phosphatases: one is the inducible DDSP specifically inactivating p38-MAPK and the others are constitutively expressed PTPs inactivating both ERK and p38-MAPK.

Acknowledgements

We would like to thank Otsuka Pharmaceutical Co. Ltd., Japan, for valuable discussions and help during the SSH screening.

References

[1] R.J. Davis, The mitogen-activated protein kinase signal transduction pathway, J. Biol. Chem. 268 (1993) 14553–14556.
[2] Z. Galcheva-Gargova, B. Derijard, I.H. Wu, R.J. Davis, An osmosensing signal transduction pathway in mammalian cells, Science 265 (1994) 806–808.
[3] J.M. Kyriakis, P. Banerjee, E. Nikolakaki, T. Dai, E.A. Rubie, M.F. Ahmad, J. Avruch, J.R. Woodgett, The stress-activated protein kinase subfamily of c-*Jun* kinases, Nature 369 (1994) 156–160.
[4] E. Cano, L.C. Mahadevan, Parallel signal processing among mammalian MAPKs, Trends Biochem. Sci. 20 (1995) 117–122.
[5] R. Seger, E.G. Krebs, The MAPK signaling cascade, FASEB J. 9 (1995) 726–735.
[6] S. Tamura, M. Hanada, M. Ohnishi, K. Katsura, M. Sasaki, T. Kobayashi, Regulation of stress-activated protein kinase signaling pathways by protein phosphatases, Eur. J. Biochem. 269 (2002) 1060–1066.
[7] J.A. McLachlan, C.D. Serkin, O. Bakouche, Dehydroepiandrosterone modulation of lipopolysaccharide-stimulated monocyte cytotoxicity, J. Immunol. 156 (1996) 328–335.
[8] T. Yoshimata, A. Yoneyama, Y. Jin-no, N. Tamai, Y. Kamiya, Effects of dehydroepiandrosterone on mitogen-activated protein kinase in human aortic smooth muscle cells, Life Sci. 65 (1999) 431–440.
[9] M.R. Williams, S. Ling, T. Dawood, K. Hashimura, A. Dai, H. Li, J.P. Liu, J.W. Funder, K. Sudhir, P.A. Komesaroff, Dehydroepiandrosterone inhibits human vascular smooth muscle cell proliferation independent of ARs and ERs, J. Clin. Endocrinol. Metab. 87 (2002) 176–181.
[10] A.J. Morales, J.J. Nolan, J.C. Nelson, S.S. Yen, Effects of replacement dose of dehydroepiandrosterone in men and women of advancing age, J. Clin. Endocrinol. Metab. 78 (1994) 1360–1367.
[11] F. Labrie, P. Diamond, L. Cusan, J.L. Gomez, A. Belanger, B. Candas, Effect of 12-month dehydroepiandrosterone replacement therapy on bone, vagina, and endometrium in postmenopausal women, J. Clin. Endocrinol. Metab. 82 (1997) 3498–3505.
[12] W. Arlt, F. Callies, J.C. van Vlijmen, I. Koehler, M. Reincke, M. Bidlingmaier, D. Huebler, M. Oettel, M. Ernst, H.M. Schulte, B. Allolio, Dehydroepiandrosterone replacement in women with adrenal insufficiency, N. Engl. J. Med. 341 (1999) 1013–1020.
[13] E.E. Baulieu, G. Thomas, S. Legrain, N. Lahlou, M. Roger, B. Debuire, V. Faucounau, L. Girard, M.P. Hervy, F. Latour, M.C. Leaud, A. Mokrane, H. Pitti-Ferrandi, C. Trivalle, O. de Lacharriere, S. Nouveau, B. Rakoto-Arison, J.C. Souberbielle, J. Raison, Y. Le Bouc, A. Raynaud, X. Girerd, F. Forette, Dehydroepiandrosterone (DHEA), DHEA sulfate, and aging: contribution of the DHEAge Study to a sociobiomedical issue, Proc. Natl. Acad. Sci. U. S. A. 97 (2000) 4279–4284.
[14] H. Nawata, T. Yanase, K. Goto, T. Okabe, K. Ashida, Mechanism of action of anti-aging DHEA-S and the replacement of DHEA-S, Mech. Ageing Dev. 123 (2002) 1101–1106.
[15] Z. Ravid, N. Goldblum, R. Zaizov, M. Schlesinger, T. Kertes, J. Minowada, W. Verbi, M. Greaves, Establishment and characterization of a new leukaemic T-cell line (Peer) with an unusual phenotype, Int. J. Cancer 25 (1980) 705–710.
[16] T. Okabe, M. Haji, R. Takayanagi, M. Adachi, K. Imasaki, F. Kurimoto, T. Watanabe, H. Nawata, Up-regulation of high-affinity dehydroepiandrosterone binding activity by dehydroepiandrosterone in activated human T lymphocytes, J. Clin. Endocrinol. Metab. 80 (1995) 2993–2996.
[17] J.N. Siegel, R.D. Klausner, U.R. Rapp, L.E. Samelson, T cell antigen receptor engagement stimulates c-raf phosphorylation and induces c-raf-associated kinase activity via a protein kinase C-dependent pathway, J. Biol. Chem. 265 (1990) 18472–18480.
[18] M. Izquierdo, S. Bowden, D. Cantrell, The role of Raf-1 in the regulation of extracellular signal-regulated kinase 2 by the T cell antigen receptor, J. Exp. Med. 180 (1994) 401–406.
[19] M. Adachi, M. Sekiya, M. Isobe, Y. Kumura, Z. Ogita, Y. Hinoda, K. Imai, A. Yachi, Molecular cloning and chromosomal mapping of a human protein–tyrosine phosphatase LC-PTP, Biochem. Biophys. Res. Commun. 186 (1992) 1607–1615.
[20] B. Zanke, H. Suzuki, K. Kishihara, L. Mizzen, M. Minden, A. Pawson, T.W. Mak, Cloning and expression of an inducible lymphoid-specific, protein tyrosine phosphatase (HePTPase), Eur. J. Immunol. 22 (1992) 235–239.
[21] M. Saxena, S. Williams, K. Tasken, T. Mustelin, Crosstalk between cAMP-dependent kinase and MAP kinase through a protein tyrosine phosphatase, Nat. Cell Biol. 1 (1999) 305–311.
[22] M. Adachi, T. Miyachi, M. Sekiya, Y. Hinoda, A. Yachi, K. Imai, Structure of the human LC-PTP (HePTP) gene: similarity in genomic organization within protein-tyrosine phosphatase genes, Oncogene 9 (1994) 3031–3035.
[23] F. Labrie, A. Belanger, J. Simard, L.-T. Van, C. Labrie, DHEA and peripheral androgen and estrogen formation: intracinology, Ann. N.Y. Acad. Sci. 774 (1995) 16–28.
[24] R.H. Derksen, Dehydroepiandrosterone (DHEA) and systemic lupus erythematosus, Semin. Arthritis Rheum. 27 (1998) 335–347.
[25] D.M. Chang, J.L. Lan, H.Y. Lin, S.F. Luo, Dehydroepiandrosterone treatment of women with mild-to-moderate systemic lupus erythematosus: a multicenter randomized, double-blind, placebo-controlled trial, Arthritis Rheum. 46 (2002) 2924–2927.
[26] M.A. Petri, R.G. Lahita, R.F. Van Vollenhoven, J.T. Merrill, M. Schiff, E.M. Ginzler, V. Strand, A. Kunz, K.J. Gorelick, K.E. Schwartz, Effects of prasterone on corticosteroid requirements of women with systemic lupus erythematosus: a double-blind, randomized, placebo-controlled trial, Arthritis Rheum. 46 (2002) 1820–1829.
[27] R.F. van Vollenhoven, Dehydroepiandrosterone in systemic lupus erythematosus, Rheum. Dis. Clin. North Am. 26 (2000) 349–362.
[28] A.C. Grammer, R. Fischer, O. Lee, X. Zhang, P.E. Lipsky, Flow cytometric assessment of the signaling status of human B lymphocytes from normal and autoimmune individuals, Arthritis Res. Ther. 6 (2004) 28–38 (Electronic publication 2004 Feb 2005).
[29] R.L. Thurmond, S.A. Wadsworth, P.H. Schafer, R.A. Zivin, J.J. Siekierka, Kinetics of small molecule inhibitor binding to p38 kinase, Eur. J. Biochem. 268 (2001) 5747–5754.
[30] H. Shimizu, M. Shiota, N. Yamada, K. Miyazaki, N. Ishida, S. Kim, H. Miyazaki, Low M(r) protein tyrosine phosphatase inhibits growth and migration of vascular smooth muscle cells induced by platelet-derived growth factor, Biochem. Biophys. Res. Commun. 289 (2001) 602–607.
[31] M.E. Poynter, R.A. Daynes, Peroxisome proliferator-activated receptor alpha activation modulates cellular redox status, represses nuclear factor-kappaB signaling, and reduces inflammatory cytokine production in aging, J. Biol. Chem. 273 (1998) 32833–32841.
[32] R. Dashtaki, A.R. Whorton, T.M. Murphy, P. Chitano, W. Reed, T.P. Kennedy, Dehydroepiandrosterone and analogs inhibit DNA binding of AP-1 and airway smooth muscle proliferation, J. Pharmacol. Exp. Ther. 285 (1998) 876–883.
[33] D. Liu, J.S. Dillon, Dehydroepiandrosterone activates endothelial cell nitric-oxide synthase by a specific plasma membrane receptor coupled to Galpha(i2,3), J. Biol. Chem. 277 (2002) 21379–21388 (Electronic publication 22002 Apr 21304).
[34] M. Saxena, S. Williams, J. Brockdorff, J. Gilman, T. Mustelin, Inhibition of T cell signaling by mitogen-activated protein kinase-

targeted hematopoietic tyrosine phosphatase (HePTP), J. Biol. Chem. 274 (1999) 11693–11700.
[35] M. Oh-hora, M. Ogata, Y. Mori, M. Adachi, K. Imai, A. Kosugi, T. Hamaoka, Direct suppression of TCR-mediated activation of extracellular signal-regulated kinase by leukocyte protein tyrosine phosphatase, a tyrosine-specific phosphatase, J. Immunol. 163 (1999) 1282–1288.
[36] S.M. Pettiford, R. Herbst, The MAP-kinase ERK2 is a specific substrate of the protein tyrosine phosphatase HePTP, Oncogene 19 (2000) 858–869.
[37] M. Camps, A. Nichols, S. Arkinstall, Dual specificity phosphatases: a gene family for control of MAP kinase function, FASEB J. 14 (2000) 6–16.
[38] A. Gjorloff-Wingren, M. Saxena, S. Han, X. Wang, A. Alonso, M. Renedo, P. Oh, S. Williams, J. Schnitzer, T. Mustelin, Subcellular localization of intracellular protein tyrosine phosphatases in T cells, Eur. J. Immunol. 30 (2000) 2412–2421.
[39] M. Saxena, S. Williams, J. Gilman, T. Mustelin, Negative regulation of T cell antigen receptor signal transduction by hematopoietic tyrosine phosphatase (HePTP), J. Biol. Chem. 273 (1998) 15340–15344.
[40] M. Fiscella, H. Zhang, S. Fan, K. Sakaguchi, S. Shen, W.E. Mercer, G.F. Vande Woude, P.M. O'Connor, E. Appella, Wip1, a novel human protein phosphatase that is induced in response to ionizing radiation in a p53-dependent manner, Proc. Natl. Acad. Sci. U. S. A. 94 (1997) 6048–6053.
[41] M. Takekawa, M. Adachi, A. Nakahata, I. Nakayama, F. Itoh, H. Tsukuda, Y. Taya, K. Imai, p53-inducible wip1 phosphatase mediates a negative feedback regulation of p38 MAPK-p53 signaling in response to UV radiation, EMBO J. 19 (2000) 6517–6526.

0021-972X/05/$15.00/0
Printed in U.S.A.

The Journal of Clinical Endocrinology & Metabolism 90(5):2508–2511

doi: 10.1210/jc.2004-2067

Subtle 17α-Hydroxylase/17,20-Lyase Deficiency with Homozygous Y201N Mutation in an Infertile Woman

Matsuo Taniyama, Makito Tanabe, Hiroshi Saito, Yoshio Ban, Hajime Nawata, and Toshihiko Yanase

Division of Endocrinology and Metabolism, Departments of Internal Medicine (M.Tani) and Obstetrics and Gynecology (H.S.), Showa University Fujigaoka Hospital, Yokohama 227-8501, Japan; Third Department of Internal Medicine (M.Tani., Y.B.), Showa University School of Medicine, Tokyo 142-8666, Japan; and Third Department of Internal Medicine (M.Tana., H.N., T.Y.), Faculty of Medicine, Kyushu University, Fukuoka 818-8582, Japan

Steroid 17α-hydroxylase deficiency is characterized by failed sexual development and mineralocorticoid hypertension. Female patients usually exhibit primary amenorrhea. Some patients with partial deficiency are reported to have menses, yet they have hypertension and hypokalemia. We describe here a normotensive, infertile female patient with menses and minimal defects in secondary sex characteristics.

The patient experienced menarche at age 13, and her menstrual cycles were regular until age 18 and irregular thereafter. Pubic hair was present (Tanner stage 3), and breast maturation was within normal range (Tanner stage 5). The patient's resting blood pressure was normal, and hypokalemia was not observed despite high blood corticosterone levels and reduced plasma renin activity. Analysis of the CYP17 gene revealed that the patient was homozygous for the Y201N mutation. *In vitro* expression of the mutated Y201N enzyme revealed reduced activities of both 17α-hydroxylase and 17,20-lyase; however, these reductions were less than those of the F53/54DEL mutation, which also shows mild clinical deficiency of 17α-hydroxylase/17,20-lyase. Thus, the 17α-hydroxylase/17,20-lyase deficiency in the present case is very mild both clinically and enzymatically. This case raises the possibility that there are infertile, menstruating women with undiagnosed 17α-hydroxylase deficiency. (*J Clin Endocrinol Metab* 90: 2508–2511, 2005)

STEROID 17α-HYDROXYLASE DEFICIENCY (17OHD) is an autosomal recessive disorder characterized by failure of sexual development and mineralocorticoid hypertension (1–4). It is caused by a defect (5) in the steroidogenic enzyme cytochrome P450c17 gene (6), which has both 17α-hydroxylase and 17,20-lyase activities. Lack of sex steroids results in female external genitalia in genetically male individuals and the absence of sexual maturation, including primary amenorrhea, in genetically female individuals (7). Mineralocorticoid excess causes severe hypertension and hypokalemia. In a milder form of 17OHD, genetically male individuals exhibit ambiguous genitalia (8–10), and female patients sometimes menstruate (11, 12). Most patients with mild 17OHD have severe hypertension. When defects in the secondary sexual characteristics are minimal and severe hypertension is absent in female patients who menstruate, 17OHD may be overlooked.

We observed subtle 17OHD in a female patient with minimal defects in sexual maturation and detected a mutation in the CYP17 gene. This case suggests that there may be undiagnosed cases of mild 17OHD among normotensive menstruating women.

Patient and Methods

Clinical features

The patient was a 38-yr-old Japanese woman who was evaluated for low plasma renin activity. She was an offspring of a consanguineous marriage. She had menarche at age 13, and her menstrual cycles were regular until age 18 and irregular thereafter. After marriage, she was found to be infertile and was under the care of an obstetric clinic for several years. She visited Showa University Hospital at age 34 because of atypical genital bleeding. Her blood pressure at that time was 130/84. On gynecological examination, hypoplastic uterus was observed. Plasma LH and FSH levels were 17 and 22 mU/ml, respectively. Serum progesterone was 2.2 ng/ml, and serum estradiol was 107 pg/ml.

Four years later, when she visited the Division of Internal Medicine, her initial blood pressure was 156/80. It rose to 180/100 in the doctor's presence and then dropped to 150/90 after several deep breaths. Self-monitoring of blood pressure at home showed her regular blood pressure to be 120–130/70–80; however, it did increase in response to stress. Thereafter, her blood pressure at each visit to the outpatient clinic was almost normal. Although her initial hypertension was thought to be a form of white-coat hypertension, laboratory tests revealed that both plasma renin activity and aldosterone concentration were low, which prompted further endocrinological evaluations. She was 157 cm tall and weighed 45 kg. Pubic hair was present but relatively scarce (Tanner stage 3). Axillary hair had been present but was almost absent at the time of examination. Breast maturation was within normal limits (Tanner stage 5). Her karyotype was 46XX. Serum potassium concentrations were always within normal range. The patient's serum steroid hormone profile is shown in Table 1. A marked increase in corticosterone and a slight increase in deoxycorticosterone were observed. These steroid levels were markedly reduced with dexamethasone administration. Serum cortisol levels and plasma ACTH level were within normal limits, but the cortisol level did not respond well to ACTH load. Serum dehydroepiandrosterone sulfate was within the normal range, and serum androstenedione was low. Abdominal computed tomography revealed no adrenal tumor or hypertrophy of the adrenal glands.

Sequence analysis

Genomic DNA was extracted from peripheral blood leukocytes. The coding regions of exons 1–8 of the CYP17 gene, including exon-intron boundaries, were amplified from 1 μg genomic DNA by PCR with a set of gene-specific primers as described previously (13). Nucleotide sequences of purified PCR products were determined by direct sequencing

First Published Online February 15, 2005

Abbreviations: 17OHD, 17-Hydroxylase deficiency; RFLP, restriction fragment length polymorphism.

TABLE 1. Hormonal data

	Normal range	Basal	After dexa	ACTH load, 60 min
PRA (ng/ml·h)	0.20–3.90	<0.15–0.47		
Aldosterone (ng/dl)	3.6–24.0	2.3–6.7		
Progesterone (ng/ml)	<1.7	2.2–5.9	0.3	7.4
DOC (ng/ml)	0.11–0.40	0.40–0.59	0.04	1.0
Corticosterone (ng/ml)	0.21–8.48	23.8–132.0	3.0	312.0
18-OH DOC (ng/ml)	0.01–0.07	0.26		
17-OHP (ng/ml)	0.2–4.5	0.2	<0.1	1.0
Cortisol (μg/dl)	4.0–18.3	5.5–12.4		14.0
DHEA-S (ng/ml)	640–2030	769–1090		
Androstenedione (ng/ml)	0.6–2.2	0.2		
Estradiol (pg/ml)	10–366	90–333		
ACTH (pg/ml)	8.2–54.8	40		
LH (mIU/ml)	1.7–19.8	17–23		
FSH (mIU/ml)	1.1–13.6	22–33		
K (mEq/liter)	3.5–4.8	3.8–4.2		

Basal values with ranges are the results of multiple measurements. After dexa, overnight after 1 mg dexamethasone administration; PRA, plasma renin activity; DOC, deoxycorticosterone; 17-OHP, 17-hydroxyprogesterone; DHEA-S, dehydroepiandrosterone sulfate.

with an ABI Prism Dye Termination Cycle Sequencing Core Kit (Applied Biosystems, Foster City, CA).

PCR-restriction fragment length polymorphism (PCR-RFLP) analysis

The detected mutation eliminates a *Tsp*E1 restriction site. We performed PCR-RFLP analysis of genomic DNA from the patient and her parents. The mutated codon was amplified with primers 5′-GGCCAC-CCACAACGGACAGTC-3′ and 5′-GACTAGGTCCACCAGGCTGTC-3′. PCR consisted of 33 cycles of 94 C for 1 min, 58 C for 1 min, and 72 C for 1 min. PCR products were purified by ethanol precipitation, digested with *Tsp*E1 at 65 C for 4 h, and separated by agarose gel.

Site-directed mutagenesis, transfection of COS1 cells, and enzyme assays

A detected mutation was created in a human P450c17 cDNA in Bluescript (pBSH 17α-1), which was produced previously by Yanase *et al.* (14). Site-directed mutagenesis was performed with a BD Transformer Site-Directed Mutagenesis Kit (BD Biosciences Clontech, Tokyo, Japan) with a primer designed for the nucleotide change. The full-length mutant cDNA was sequenced to confirm the mutation. The *Bam*HI-*Hin*dIII fragment containing the full-length mutant cDNA was inserted into the pCMV expression vector at the *Bgl*II and *Hin*dIII sites.

Transfection of COS-1 cells and thin layer chromatography analysis of the catalytic properties of P450c17 were carried out as described previously (14). Enzyme activities were compared with those of wild-type enzyme, which was produced with pCMV17α-H, and another mutant with mild 17α-hydroxylase/17,20-lyase deficiency, F53/54DEL enzyme, which was produced with pCMVJG17α-H (14). Immunoblotting of cellular proteins with antibody raised against porcine testis P450c17 was carried out as previously described (14).

Results

Sequence of the CYP17 gene

A homozygous T→A transversion at nucleotide position 2472 in exon 3 of CYP17 (amino acid change, Tyr201 to Asn:Y201N) was detected in the proband (Fig. 1).

PCR-RFLP analysis

Because the T2472A mutation eliminates a *Tsp*E1 restriction site, we used PCR-RFLP analysis for genotyping (Fig. 2).

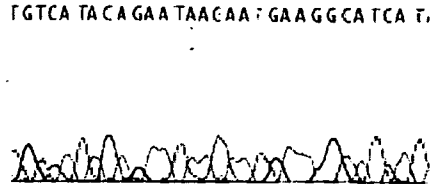

FIG. 1. Sequence analysis of the CYP17 gene revealed homozygous mutation of thymine to adenine at nucleotide position 2472 in exon 3, which causes amino acid substitution tyrosine 201 to asparagine (Y201N).

The expected PCR product was 184 bp. Digestion of the wild-type allele with *Tsp*E1 yielded 127-bp and 57-bp fragments. The patient carried only the mutant allele, whereas both her parents were heterozygous for the mutant allele.

In vitro expression study

To determine the functional significance of the Y201N mutation, the mutant cDNA was cloned into a eukaryotic expression vector, pCMV, and expressed in nonsteroidogenic COS-1 cells. Cells expressing the mutant cDNA(Y201N) produced the same amount of immunodetectable P450c17 protein as cells expressing wild-type P450c17 cDNA or mutant P450c17 cDNA (F53/54DEL) (data not shown). Although there was a similar amount of immunodetectable P450c17 protein in the various transfectants, the activities of P450c17 (Y201N), including 17α-hydroxylation and 17,20-lyase activity, were reduced. Comparison of the initial kinetics with progesterone and 17α-hydroxypregnenolone as substrates revealed that the 17α-hydroxylase and 17,20-lyase activities of P450c17 (Y201N) were less than 33% and less than 35%, respectively, those of wild-type P450c17. The activities of P450c17 (F53/54DEL) were less than 22 and 5.2%, respectively, those of wild-type (Table 2). Thus, P450c17 (Y201N) had greater 17α-hydroxylase and 17,20-lyase activities than did P450c17 (F53/54DEL), and both were reduced in parallel in P450c17 (Y201N), whereas there was a much greater reduction of 17,20-lyase activity relative to 17α-hydroxylase activity in P450c17 (F53/54DEL), as previously observed (14).

Discussion

The degree of deficiency in 17α-hydroxylase and 17,20-lyase activities in the present case was very mild. The manifestations possibly related to the enzyme defect were lack of

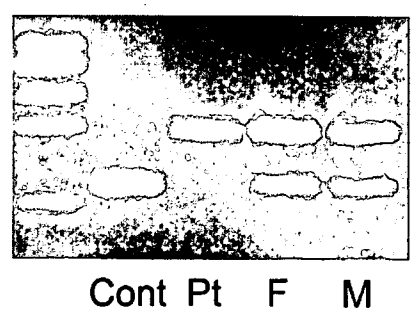

FIG. 2. PCR-RFLP analysis. Y201N mutation eliminates a *Tsp*E1 restriction site. Cont, Control; Pt, patient; F, father; M, mother. Patient had two mutant alleles, whereas each parent had one normal allele and one mutant allele.

TABLE 2. Enzymatic activities of mutant enzymes

	17α-hydroxylase (%)	17,20-lyase (%)
Wild type	180.5 (100)	73.3 (100)
Y201N	56.5 (31.3)	24.8 (33.7)
F53/54DEL	37.8 (20.9)	3.8 (5.2)

All values are the mean of two independent measurements. Units for all measurements are picomoles per dish.

axillary hair, irregular menstruation, hypoplastic uterus, infertility, and occasional hypertension. However, biochemical analyses suggested that the patient had 17OHD. Plasma renin activity and aldosterone level were low, whereas plasma corticosterone was high and suppressed by dexamethasone. We were not sufficiently confident to diagnose 17OHD at that time because hypokalemia was absent and plasma cortisol and corticotropin levels were within normal limits. Because consanguinity supported recessive inheritance, we sequenced the CYP17 gene and found that the proband was homozygous for a novel missense mutation. Each parent carried one mutant allele. *In vitro* expression analysis revealed that the Y201N mutation partially reduces the activities of both 17α-hydroxylase and 17,20-lyase. The 17α-hydroxylase activity and 17,20-lyase activity of mutant P450c17 were less than 33% and less than 35%, respectively, those of wild-type P450c17. This finding is consistent with the patient's clinical 17α-hydroxylase/17,20-lyase activities. It appears that a 17α-hydroxylase activity that is 30% of that of normal may be sufficient to maintain a normal blood pressure. The patient's 17,20-lyase activity (30% of normal) was higher than a previously reported patient with the F53/54DEL mutation, whose 17,20-lyase activity was 5% of that of normal and with regular menstruation (14). Therefore, this mutant may allow for regular menstruation. Although Tyr201 is located in the F helix that forms the F-G loop, the structural and functional significance of this region of the molecule remains unclear (15).

The clinical manifestations of 17α-hydroxylase/17,20-lyase deficiency reflect the activities of the mutated enzymes. Mutations that result in complete loss of enzymatic activities yield the phenotypes associated with complete deficiency (16). Partial deficiency is related to mutations that only partially affect activities (10, 17). Isolated 17,20-lyase deficiency, in which only phenotypes related to sex hormone deficiency are present and those of mineralocorticoid excess are absent, is caused by specific mutations such as R347H and R358Q (18). These mutations cause only 17,20-lyase defects, and 17α-hydroxylase activity is essentially unaffected (19).

There are generally three opportunities for diagnosis of 17OHD. Ambiguous genitalia at birth give the opportunity to check for genetically male infants with partial deficiency. Genetically male individuals with severe deficiency and genetically female individuals are both phenotypically female, and sex hormone deficiencies are typically recognized at puberty. Primary amenorrhea and lack of female secondary sex characteristics, including breast development and pubic hair, may require evaluation. In other cases, the disease is detected during the course of evaluation of severe hypertension. Genetic females with 17OHD who menstruate are typically identified in this manner (11, 12). To date, approximately 10 patients with 17OHD and menstruation have been reported including three patients with homozygous F53/54DEL mutation (Refs. 11, 12, 21, 22, and references in Ref. 2). Although these patients menstruated, only three had pubic hair and mature breast development. Moreover, with the exception of the patient described herein, all had severe hypertension and hypokalemia. Cases of 17OHD without hypertension (Ref. 23 and references in Ref. 2) or with mild hypertension (7) have been reported; however, the patients had primary amenorrhea. Thus, our case appears to be very rare. However, mild cases may be overlooked because the patients are not evaluated for mineralocorticoid excess or sex hormone deficiencies. Such infertile patients with mild 17OHD have been reported (24). Some specific mutations are reported to be widespread in the particular geographic area (25). It is conceivable that undiagnosed patients with subtle 17OHD with mild deficiency of enzyme activities are present.

It was reported that administration of testosterone as an aromatizable substrate to a patient with 17OHD resulted in follicular maturation and ovulation (26). Thus, identification of 17OHD is essential not only for diagnosis of the cause of infertility but also for developing possible strategies to treat this type of infertility. It seems valuable to screen for 17OHD by plasma renin activity or by corticosterone or progesterone level (27) in infertile women with only minimal defects on sexual maturation.

Acknowledgments

Received October 19, 2004. Accepted February 4, 2005.

Address all correspondence and requests for reprints to: Matsuo Taniyama, M.D., Division of Endocrinology and Metabolism, Department of Internal Medicine, Showa University Fujigaoka Hospital, 1-30 Fujigaoka, Aoba, Yokohama, Kanagawa 227-8501, Japan. E-mail: taniyama@showa-university-fujigaoka.gr.jp.

References

1. **Biglieri EG, Herron MA, Brust N** 1966 17-Hydroxylation deficiency in man. J Clin Invest 45:1946–1954
2. **Yanase T, Simpson ER, Waterman MR** 1991 17α-Hydroxylase/17,20-lyase deficiency: from clinical investigation to molecular definition. Endocr Rev 12:91–108
3. **Kater CE, Biglieri EG** 1994 Disorders of steroid 17α-hydroxylase deficiency. Endocrinol Metab Clin North Am 23:341–357
4. **Auchus RJ** 2001 The genetics, pathophysiology, and management of human deficiencies of P450c17. Endocrinol Metab Clin North Am 30:101–119
5. **Kagimoto M, Winter JS, Kagimoto K, Simpson ER, Waterman MR** 1988 Structural characterization of normal and mutant human steroid 17α-hydroxylase genes: molecular basis of one example of combined 17α-hydroxylase/17,20 lyase deficiency. Mol Endocrinol 2:564–570
6. **Picardo-Leonard J, Miller WL** 1987 Cloning and sequence of the human gene for $P450_{C17}$ (steroid 17α-hydroxylase/17,20 lyase): similarity with the gene for $P450_{C21}$. DNA 6:439–448
7. **Nagamani M, Dinh TV** 1986 17α-Hydroxylase deficiency in genetic females. A report of two cases. J Reprod Med 31:734–738
8. **New MI** 1970 Male pseudohermaphroditism due to 17α-hydroxylase deficiency. J Clin Invest 49:1930–1941
9. **Dean HJ, Shackleton CH, Winter JS** 1984 Diagnosis and natural history of 17-hydroxylase deficiency in a newborn male. J Clin Endocrinol Metab 59: 513–520
10. **Ahlgren R, Yanase T, Simpson ER, Winter JS, Waterman MR** 1992 Compound heterozygous mutations (Arg 239→stop, Pro 342→Thr) in the *CYP17* (P45017α) gene lead to ambiguous external genitalia in a male patient with partial combined 17α-hydroxylase/17,20-lyase deficiency. J Clin Endocrinol Metab 74:667–672
11. **Miura K, Yasuda K, Yanase T, Yamakita N, Sasano H, Nawata H, Inoue M, Fukaya T, Shizuta Y** 1996 Mutation of cytochrome P-45017α gene (CYP17) in a Japanese patient previously reported as having glucocorticoid-responsive

hyperaldosteronism: with a review of Japanese patients with mutations of CYP17. J Clin Endocrinol Metab 81:3797–3801
12. **Singhellakis PN, Panidis D, Papadimas J, Demertzi H, Tsourdis A, Sotsiou F, Ikkos DG** 1986 Spontaneous sexual development and menarche in a female with 17α-hydroxylase deficiency. J Endocrinol Invest 9:177–183
13. **Lin D, Harikrishna JA, Moore CCD, Jones KL, Miller WL** 1991 Missense mutation serine106→proline causes 17α-hydroxylase deficiency. J Biol Chem 266:15992–15998
14. **Yanase T, Kagimoto M, Suzuki S, Hashiba K, Simpson ER, Waterman MR** 1989 Deletion of a phenylalanine in the N-terminal region of human cytochrome $P\text{-}450_{17\alpha}$ results in partial combined 17α-hydroxylase/17,20-lyase deficiency. J Biol Chem 264:18076–18082
15. **Auchus RJ, Miller WL** 1999 Molecular modeling of human P450c17 (17α-hydroxylase/17,20-lyase): insights into reaction mechanisms and effects of mutations. Mol Endocrinol 13:1169–1182
16. **Yanase T** 1995 17α-Hydroxylase/17,20-lyase defects. J Steroid Biochem Mol Biol 53:153–157
17. **Laflamme N, Leblanc JF, Mailloux J, Faure N, Labrie F, Simard J** 1996 Mutation R96W in cytochrome P450c17 gene causes combined 17α-hydroxylase/17–20-lyase deficiency in two French Canadian patients. J Clin Endocrinol Metab 81:264–268
18. **Geller DH, Auchus RJ, Mendonca BB, Miller WL** 1997 The genetic and functional basis of isolated 17,20-lyase deficiency. Nat Genet 17:201–205
19. **Geller DH, Auchus RJ, Miller WL** 1999 P450c17 mutations R347H and R358Q selectively disrupt 17,20-lyase activity with P450 oxidoreductase and cytochrome b_5. Mol Endocrinol 13:167–175
20. **Kaneko E, Kobayashi Y, Yasukochi Y, Kishi Y, Numano F** 1994 Genomic analysis of two siblings with 17α-hydroxylase deficiency and hypertension. Hypertens Res 17:143–147
21. **Oshiro C, Takasu N, Wakugami T, Komiya I, Yamada T, Eguchi Y, Takei H** 1995 Seventeen α-hydroxylase deficiency with one base pair deletion of the cytochrome P450c17 (*CYP17*) gene. J Clin Endocrinol Metab 80:2526–2529
22. **Katayama Y, Kado S, Wada S, Nemoto Y, Kugai N, Furuya K, Nagata N** 1994 A case of 17α-hydroxylase deficiency with retained menstruation. Endocr J 41:213–218
23. **Satoh J, Kuroda Y, Nawata H, Yanase T** 1998 Molecular basis of hypokalemic myopathy caused by 17α-hydroxylase/17,20-lyase deficiency. Neurology 51: 1748–1751
24. **Levran D, Ben-Shlomo I, Pariente C, Dor J, Mashiach S, Weissman A** 2003 Familial partial 17,20-desmolase and 17α-hydroxylase deficiency presenting as infertility. J Assist Reprod Genet 20:21–28
25. **Costa-Santos M, Kater CE, Auchus RJ, Brazilian Congenital Adrenal Hyperplasia Multicenter Study Group** 2004 Two prevalent *CYP17* mutations and genotype-phenotype correlations in 24 Brazilian patients with 17-hydroxylase deficiency. J Clin Endocrinol Metab 89:49–60
26. **Neuwinger J, Licht P, Munzer B, Sir-Petermann T, Siebzehnrubl E, Wildt L** 1996 Substitution with testosterone as aromatizable substrate for induction of follicular maturation, estradiol production and ovulation in a patient with 17α-hydroxylase deficiency. Exp Clin Endocrinol Diabetes 104:400–408
27. **Martin RM, Lin CJ, Costa EM, de Oliveira ML, Carrilho A, Villar H, Longui CA, Mendonca BB** 2003 P450c17 deficiency in Brazilian patients: biochemical diagnosis through progesterone levels confirmed by *CYP17* genotyping. J Clin Endocrinol Metab 88:5739–5746

JCEM is published monthly by The Endocrine Society (http://www.endo-society.org), the foremost professional society serving the endocrine community.

0021-972X/05/$15.00/0
Printed in U.S.A.

The Journal of Clinical Endocrinology & Metabolism 90(11):6162–6169

doi: 10.1210/jc.2005-0179

Impaired Nuclear Translocation, Nuclear Matrix Targeting, and Intranuclear Mobility of Mutant Androgen Receptors Carrying Amino Acid Substitutions in the Deoxyribonucleic Acid-Binding Domain Derived from Androgen Insensitivity Syndrome Patients

Hisaya Kawate, Yin Wu, Keizo Ohnaka, Rong-Hua Tao, Kei-ichiro Nakamura, Taijiro Okabe, Toshihiko Yanase, Hajime Nawata, and Ryoichi Takayanagi

Departments of Geriatric Medicine (H.K., Y.W., K.O., R.-H.T., R.T.) and Medicine and Bioregulatory Science (T.O., T.Y., H.N.), Graduate School of Medical Sciences, Kyushu University, Fukuoka 812-8582, Japan; and Department of the Second Anatomy (K.N.), Kurume University School of Medicine, Kurume, 830-0011, Japan

Context: Recent imaging studies revealed that androgen receptor (AR) is ligand-dependently translocated from the cytoplasm into the nucleus and forms intranuclear fine foci. In this study, we examined whether intracellular dynamics of mutant ARs detected in two androgen insensitivity syndrome (AIS) patients was impaired.

Objective: ARs with mutations in the DNA-binding domain were functionally characterized and compared with the wild-type AR.

Patients: In a complete AIS patient (subject 1), cysteine residue 579 in the first zinc finger motif of AR was substituted for phenylalanine (AR-C579F). Another mutation (AR-F582Y) was found in a partial AIS patient (subject 2).

Results: AR-F582Y retained less than 10% of the transactivation activity of the wild-type AR, whereas no ligand-dependent transactivation was detected for AR-C579F. Image analyses of the receptors fused to green fluorescent protein showed that the wild-type AR was ligand-dependently translocated into the nucleus in which it formed fine subnuclear foci. Surprisingly, after the addition of dihydrotestosterone, the two mutant ARs initially formed large cytoplasmic dots, many of which were found to be close to mitochondria by electron microscopy. Subsequently, a part of the ligand-bound mutant ARs gradually entered the nucleus to form a smaller number of larger dots, compared with the wild-type AR. Fluorescence recovery after photobleaching analysis revealed that the intranuclear mobility of the mutant ARs decreased, compared with that of the wild-type AR.

Conclusions: These results suggest that the abnormal translocation, localization, and mobility of the mutant ARs may be the cause of AIS in these subjects. (***J Clin Endocrinol Metab* 90: 6162–6169, 2005**)

ANDROGENS PLAY AN essential role in the expression of the male phenotype. The actions of androgens are mainly mediated by the androgen receptor (AR). The AR belongs to the nuclear receptor superfamily, a large group of transcription factors whose members share basic structural and functional homology (1, 2). The N-terminal domain of the AR contains the major transactivation function region, AF-1, which acts in a ligand-independent fashion. The centrally located DNA-binding domain (DBD) is highly conserved among steroid hormone receptors and consists of two zinc finger clusters. The first zinc finger motif is involved in direct DNA-binding and contains the P-box for specific recognition of the androgen-responsive elements of target genes (3). The C-terminal ligand-binding domain (LBD) contains transactivation function domain 2 and functionally interacts with intermediary factors and nuclear cofactors. In the absence of an agonist, the LBD is believed to prevent the transactivation function of the N-terminal domain through an intramolecular interaction (4).

Unliganded ARs are located in the cytoplasm, in which they are sequestered with heat shock proteins. After ligand binding, a conformational change of the receptor protein results in unmasking of both the dimerization motif and the nuclear localization signal that allows translocation into the nucleus (1). Upon nuclear entry, the ligand-receptor complexes appear to move into subnuclear compartments, which are common congregation sites for steroid hormone receptors and other associated factors, such as nuclear receptor coactivators, that are required for transcriptional activation of the target genes. Complete subnuclear foci formation seems to be essential for steroid hormone receptor-mediated transactivation (4–6).

Because the human AR gene is located on the X chromosome at Xq11–12 (1, 4, 7), just a single allele mutation in the AR gene causes dysfunction of the receptor in 46, XY individuals, resulting in androgen insensitivity syndrome (AIS) (3, 8–10). Despite a high or normal level of serum testoster-

First Published Online August 23, 2005

Abbreviations: AIS, Androgen insensitivity syndrome; AR, androgen receptor; CAIS, complete androgen insensitivity syndrome; 3D, three-dimensional; DBD, DNA-binding domain; DHT, dihydrotestosterone; FBS, fetal bovine serum; FRAP, fluorescence recovery after photobleaching; GFP, green fluorescent protein; GR, glucocorticoid receptor; LBD, ligand-binding domain; PAIS, partial androgen insensitivity syndrome; $t_{1/2}$, half-recovery time; YFP, yellow fluorescent protein.

JCEM is published monthly by The Endocrine Society (http://www.endo-society.org), the foremost professional society serving the endocrine community.

one, AIS patients show various phenotypic abnormalities of male sexual development. AIS is subdivided into three phenotypes: complete androgen insensitivity syndrome (CAIS), partial androgen insensitivity syndrome (PAIS), and mild androgen insensitivity syndrome. AR mutations that severely impair the function of the AR cause CAIS. The main phenotypic characteristics of individuals with CAIS are female external genitalia with a short, blind-ending vagina, absent Müllerian duct, and absence of pubic and axillary hair. The gender identity is that of a normal female, but testes are commonly located in either the abdomen or the inguinal area and the uterus is absent. Laboratory findings show the 46, XY karyotype, normal or increased synthesis of testosterone by the testes, and a normal or increased level of LH. PAIS patients also show female-like external genitalia, except for clitoromegaly and/or posterior labial fusion (3, 9). Although mutations responsible for AIS are spread throughout the AR gene, there are hot spots, especially at exon 5, which encodes part of the LBD (Androgen Receptor Gene Mutation Database: www.mcgill.ca/androgendb).

We previously reported two unrelated AIS patients (one CAIS and one PAIS) carrying amino acid substitutions in the first zinc finger motif of the AR-DBD (11). In the CAIS patient (subject 1), cysteine residue 579, which coordinates a zinc ion, was substituted with phenylalanine, and the mutant AR showed almost no ligand-induced transcriptional activation. On the other hand, the AR-F582Y mutant found in the PAIS patient (subject 2) showed much less transactivation than the wild-type AR. Here, to visualize any dynamic changes of the intracellular localizations of these mutant ARs, the wild-type and mutant ARs were fused with green fluorescent protein (GFP) and their intracellular movements were analyzed using a laser confocal microscope. After treatment with the ligand, the wild-type AR was translocated from the cytoplasm into the nucleus in which it formed fine subnuclear foci. In contrast, the AR-DBD mutants initially formed large cytoplasmic dots, many of which were located close to mitochondria after the addition of dihydrotestosterone (DHT), and a proportion of the proteins subsequently moved into the nucleus to become located in subnuclear bodies. The subnuclear foci of the mutant ARs were characterized by their larger size, much smaller number, and lower mobility, compared with the wild-type AR. These results indicate that the pathogenesis of AIS in these two patients may be caused by the mislocation and lower mobility of their mutant ARs.

Subjects and Methods

Subjects

Subjects 1 and 2 were diagnosed with CAIS and PAIS, respectively, and had missense mutations of Cys^{579} to Phe and Phe^{582} to Tyr, respectively. The clinical history and data of the AIS patients characterized in the present study were previously reported (11).

Cells

COS-7 monkey kidney cells were obtained from the Riken Cell Bank (Tokyo, Japan) and maintained in DMEM (Invitrogen, Carlsbad, CA) containing antibiotics and 10% fetal bovine serum (FBS; Cansera International Inc., Etobicoke, Canada).

Plasmids

The firefly luciferase reporter plasmids, pGL3-MMTV (5) and pGL3-PSA (12), and the expression vectors for AR (pCMV-AR) were prepared as previously described (13, 14). The plasmid vectors pAR-GFP (5) and pAR-CFP (6) for expression of the AR-GFP and AR-CFP fusion proteins were constructed as described previously. Expression plasmids of the mutant ARs for mammalian cells, designated pCMV-AR-C579F (from subject 1) and pCMV-AR-F582Y (from subject 2), were constructed as previously reported (11). To construct a GFP fusion protein of the mutant AR for subject 1, a *KpnI-ScaI* fragment of pCMV-AR-C579F, which contained the mutated site, was replaced with that of pAR-GFP to generate pAR-C579F-GFP. Similarly, for subject 2, a *HindIII-ScaI* fragment of pAR-GFP was replaced with that of pCMV-AR-F582Y to construct pAR-F582Y-GFP. The validity of the structure of each construct was confirmed by DNA sequencing using an ABI PRISM 377 DNA sequencer (Applied Biosystems, Foster City, CA).

Immunoblotting

COS-7 cells were seeded in 100-mm plates and incubated for 24 h in 5% CO_2 at 37 C. Five micrograms of plasmid DNA carrying the wild-type or a mutant AR was transfected into the cells using 20 μl Superfect transfection reagent (QIAGEN GmbH, Hilden, Germany). Twenty-four hours after the transfection, the cells were washed twice with PBS and then 400 μl of Nonidet P-40 lysis buffer [50 mM Tris-HCl (pH 8.0), 150 mM NaCl, and 1% Nonidet P-40] was added to each dish, followed by rocking for 30 min at 4 C. Lysates were collected by centrifugation and the protein concentrations were measured using a BCA protein assay kit (Pierce, Rockford IL). Next, 40 μg of each lysate in 1× SDS-PAGE sample buffer [2% sodium dodecyl sulfate, 100 mM dithiothreitol, 60 mM Tris-HCl (pH 6.8), and 0.01% bromophenol blue] was loaded onto a sodium dodecyl sulfate-polyacrylamide gel (10% separating gel) and electrophoresed at 20 mA for 4 h. Proteins were transferred onto nitrocellulose membrane (Hybond P; Amersham Biosciences, Piscataway, NJ) using a Trans-Blot SD Semi-Dry transfer cell (Bio-Rad Laboratories, Hercules, CA) at 250 V for 1 h at 25 C. After blocking the membrane in 1× Block-Ace (Dainippon Pharmaceutical Co., Osaka, Japan), an anti-AR polyclonal antibody (sc-816; Santa Cruz Biotechnology Inc., Santa Cruz, CA) was reacted with the membrane in 0.1× Block-Ace for 1 h at 25 C. After a brief wash with Tris-buffered saline-Tween 20 (10 mM Tris-HCl, 0.9% NaCl, and 0.05% Tween 20), horseradish peroxidase-conjugated antirabbit Ig antibodies (Amersham Biosciences) were added in 0.1× Block-Ace as the secondary antibody, and the membrane was incubated for 45 min at 25 C with gentle shaking. After washing with Tris-buffered saline-Tween 20, the membrane was reacted with Western blotting detection reagents (Amersham Biosciences) for 1 min in a dark room. The labeled protein bands were visualized and analyzed using a VersaDoc imaging system 5000 (Bio-Rad).

Functional reporter assays

COS-7 cells (1×10^5 cells/well) were seeded in 12-well plates at 20 h before transfection. Cells were cotransfected with 0.5 μg/well of pGL3-MMTV as a reporter plasmid, 2 ng/well of pRL-CMV (Promega Corp., Madison, WI) as an internal control, and 0.1 μg/well of a wild-type or mutant AR expression plasmid with 1.7 μl/well of Superfect. In all transfection experiments, the total amount of plasmid DNA was fixed by adding empty vector to the transfection mixture. At 3 h after transfection, 0.5 ml of DMEM containing 10% charcoal-treated FBS was added with or without steroid hormone (10^{-8} M DHT). After incubation for 24 h, the cells were rinsed with PBS and lysed in the lysis buffer contained in a luciferase assay kit (Promega). The luciferase activity was assayed using the dual-luciferase assay system (Promega) and a Lumat LB 9507 (Berthold Technologies, Bad Wildbad, Germany). Each value was determined as the average of three independent experiments. Data were presented as the means ± SD. One-way ANOVA followed by Scheffé's test was used for multigroup comparisons. $P < 0.05$ was considered to be statistically significant

Confocal laser-scanning microscopy

For living cell microscopy, COS-7 cells (2×10^5 cells/well) were seeded in 35-mm glass-bottom dishes (Asahi Techno Glass Corp., Tokyo,

Japan) and transfected with 0.5 μg of plasmid DNA carrying the wild-type or a mutant AR fused with GFP or yellow fluorescent protein (YFP) using 5 μl/well Superfect. The cells were maintained in DMEM supplemented with 10% charcoal-treated FBS for 20 h, and then various steroid hormones were added to the medium. The cells were observed with an Axiovert 200M inverted microscope equipped with an LSM510META scan head (Carl Zeiss, Jena, Germany) using a ×100, 1.4 numerical aperture oil immersion objective. Images were collected at a 12-bit depth resolution of intensities over 1024 × 1024 pixels. For excitation of GFP and YFP, a 488-nm argon laser was used and a series of images was obtained. The GFP and YFP signals were separated using the emission fingerprinting technique established by Carl Zeiss. Separation of the individual emission signals was based on recording a spectral signature and applying a linear unmixing algorithm using the reference spectra of each fluorescent protein (15).

To construct three-dimensional (3D) images, a series of 30–50 two-dimensional tomographic images were collected for each cell using the confocal microscope. These images were exported as TIF files and the TRI graphic program (Ratoc System Engineering, Tokyo, Japan) was used to reconstruct 3D images (6). Both the spatial distribution and calculation of the fluorescent proteins as distinct volumes were made possible by removing scattering background fluorescence and lens spherical aberrations and then separating each particle (6). The numbers of subnuclear foci determined for the wild-type and mutant ARs were representative of at least 20 cells.

Fluorescence recovery after photobleaching (FRAP) analysis

Cells were transfected with the wild-type AR and a mutant AR and incubated for 24 h at 37 C. After a further 5-h incubation with DHT, FRAP analysis was performed. After collection of the initial image using a Carl Zeiss LSM510META microscope, a selected area of a fixed size in the nucleus was photobleached by setting the laser wavelength to 488 nm and using the maximum power for 50 iterations. After the bleaching, images within the bleached region were taken every second at a resolution of 512 × 512 pixels to follow the recovery of the fluorescence intensity. The intensity of the fluorescence was calculated using the LSM510 software and the half-recovery time ($t_{1/2}$) was determined as the time when the fluorescence intensity reached half the maximal recovery using the Microsoft Excel software. Each $t_{1/2}$ was the average of six to 10 FRAP experiments.

Organelle detection

COS-7 cells were transfected with pAR-C579F-GFP. Twenty-four hours after the transfection, the cells were treated with DHT and then LysoTracker Red or MitoTracker Orange CMTMRos (Molecular Probes Inc., Eugene, OR) was added in the medium at a final concentration of 100 nM to visualize the lysosomes or mitochondria, respectively. The cells were incubated for 30 min at 37 C and then rinsed with PBS. Images were collected using the fluorescence microscope.

Immunoelectron microscopy

Twenty-four hours before transfection, COS-7 cells were seeded in a 60-mm dish. The cells were transfected with 2 μg of pAR-C579F-GFP using 3 μl of Superfect. After incubation for 20 h, the cells were treated with 10^{-8} M DHT for 1 h. After a brief wash with PBS, the cells were fixed in 0.1% glutaraldehyde in 0.1 M phosphate buffer (pH 7.4) for 30 min at 25 C. The fixed cells were scraped off the dish, centrifuged at 5000 × *g* for 10 min at 4 C and resuspended in 0.1 M phosphate buffer. After dehydration in a graded series of ethanol, the cell pellet was embedded in LR White resin and ultrathin sections were cut (16). After blocking in 0.1 M phosphate buffer containing 3% BSA, the sections were incubated with rabbit polyclonal antibodies against GFP (BD Biosciences Clontech, Mountain View, CA) at 1:1000 dilution in 0.1 M phosphate buffer at 4 C overnight, followed by incubation with colloidal gold (Ø = 15 nm)-conjugated goat antirabbit IgG (Amersham Biosciences) at 1:100 dilution. After washing with distilled water, the sections was stained with 2% uranyl acetate and lead citrate, and observed with a Hitachi H-7000 electron microscope (Hitachinaka, Japan).

Results

Previously we found two different amino acid substitutions in the DBD of ARs derived from AIS patients (11). One mutation from a CAIS patient (subject 1) occurred at Cys579 which coordinates a zinc ion in the first zinc finger motif of the AR (Fig. 1A). This residue also forms a P-box that is important for the recognition of an androgen-responsive element in target genes. The other mutation from a PAIS patient (subject 2) was found at Phe582 next to the P-box (Fig. 1A). To compare the functions of these two mutant ARs with the wild-type AR, recombinant AR proteins were expressed in COS-7 cells. Immunoblot analysis showed that the expression levels of the wild-type and mutant ARs in transfected cells were almost the same (Fig. 1B). To examine AR-mediated transcriptional activation, luciferase assays were performed using the MMTV promoter containing several hormone-responsive elements (17). For the wild-type AR,

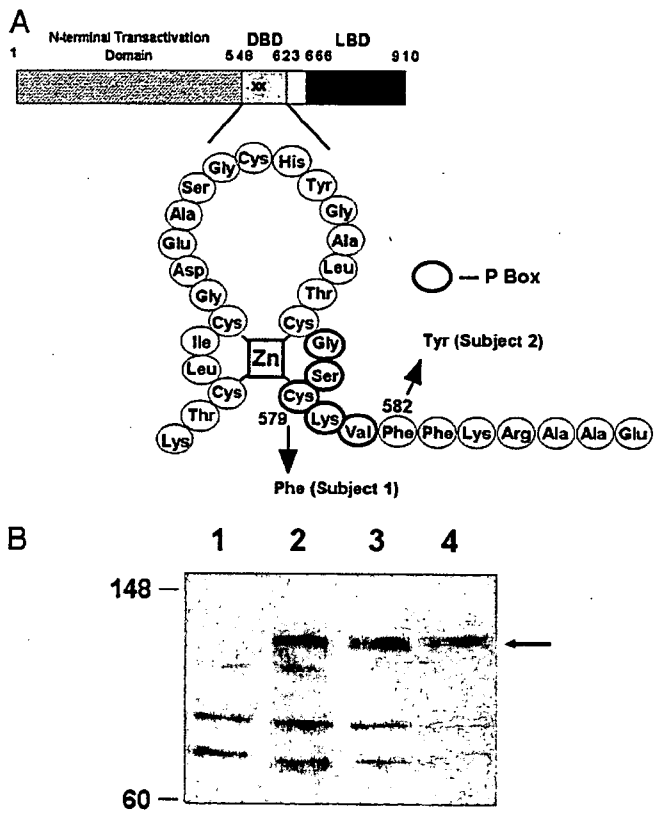

FIG. 1. The amino acid substitutions in the two AIS patients are located in the DBD of the AR. A, Schematic representation of the AR and the sites of the amino acid substitutions detected in the AIS patients. The *upper scheme* shows the domain structure of the AR: the N-terminal domain, the DBD, and the C-terminal LBD. Two different amino acid substitutions (x) were identified in the DBD of the ARs from these two AIS patients. The first zinc finger motif of the AR-DBD is magnified in the *lower scheme*. The five amino acids *circled in bold* indicate the P-box. The *arrows* indicate the amino acid substitutions in the two AIS patients. In subject 1, the cysteine at position 579 involved in the P-box is substituted by phenylalanine (C579F). In subject 2, phenylalanine 582 is changed for tyrosine (F582Y). B, Immunoblot analysis of wild-type and mutant ARs in COS-7 cells. Cells were transfected with a wild-type or mutant AR expression vector using Superfect. Twenty-four hours after the transfection, the cells were lysed and subjected to immunoblotting analysis as described in *Subjects and Methods*. Anti-AR antibodies were used for detection. The *arrow* shows the AR bands. Lane 1, Vector only; lane 2, wild-type AR; lane 3, AR-F582Y; lane 4, AR-C579F. The *numbers on the left* of the gel show the positions of protein size markers.

remarkable transcriptional activation was observed after addition of the ligand DHT. On the other hand, AR-F582Y showed less than 10% of the transcriptional activation of the wild-type AR, whereas AR-C579F showed no ligand-dependent transactivation at all (Fig. 2).

To visualize the subcellular localizations of the wild-type and mutant ARs, GFP-fusion proteins were generated and observed under a confocal laser-scanning microscope. As we previously reported, the wild-type AR was diffusely localized in the cytoplasm in the absence of the ligand (Fig. 3A) (5). Upon treatment with the ligand, the wild-type AR was almost completely translocated from the cytoplasm into the nucleus in which it formed subnuclear fine foci (Fig. 3D). The AR-DBD mutants were also diffusely present in the cytoplasm before addition of the ligand (Fig. 3, B and C). However, in contrast to the wild-type AR, the two mutant ARs formed cytoplasmic dots after the addition of DHT (Fig. 3, E and F). Time-course experiments revealed that most of the fluorescent signals for the wild-type AR were observed in the nucleus within 30 min after the addition of DHT (Fig. 4B), whereas cells expressing the AR-C579F mutant showed two patterns (Fig. 4, E–H or I–L). Approximately 80% of cells formed the cytoplasmic dots and a limited number of nuclear foci 30 min after the addition of DHT (Fig. 4F), and the nuclear dots became clear at 3 h after the ligand addition (Fig. 4H). In the other type of AR-C579F-expressing cells (20%), cytoplasmic dots were not so striking (Fig. 4J), but delayed nuclear translocation with dot formation of mutant AR was observed (Fig. 4L). In both types of the mutant-expressing cells, a smaller number of larger-sized intranuclear dots for

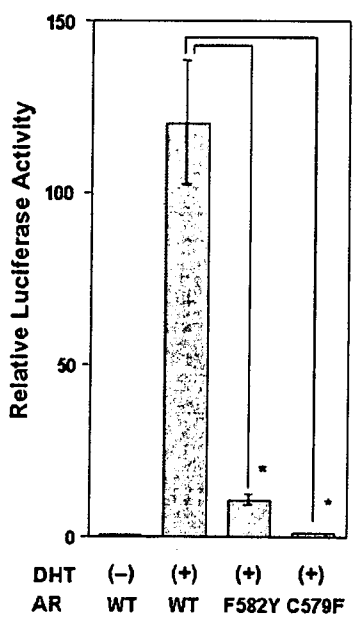

FIG. 2. Effects of the two different amino acid substitutions in the AR-DBD on transcriptional activation. COS-7 cells were transiently transfected with plasmid DNA expressing the wild-type (WT) or a mutant (C579F or F582Y) AR, pGL3-MMTV as a reporter plasmid, and pRL-CMV as an internal control. After treatment with or without 10^{-8} M DHT for 24 h, the luciferase activity was measured. The *bars* show the luciferase activities of the transfected cells relative to the value of the wild-type AR without DHT. The means ± SD of three independent experiments are shown. *, $P < 0.05$.

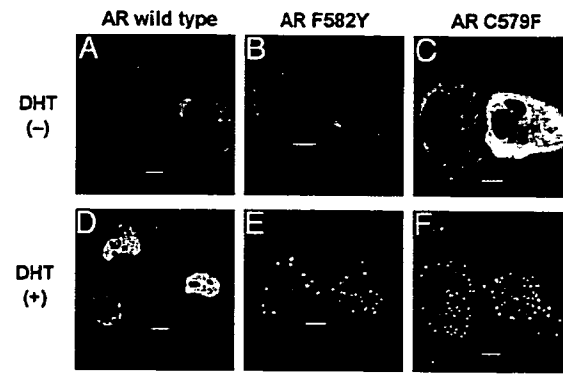

FIG. 3. Ligand-dependent translocation of the wild-type and mutant ARs. COS-7 cells were transfected with 0.5 μg of each plasmid DNA expressing GFP-fused wild-type AR (A and D), AR-F582Y (B and E), or AR-C579F (C and F). Fluorescent signals were observed at 24 h after the transfection under a laser confocal microscope (A–C). Subsequently 10^{-8} M DHT was added and incubated at 37 C for 1 h and the ligand-bound receptor proteins were observed (D–F). *Scale bar*, 10 μm.

AR-C579F were observed, compared with those for the wild-type AR (Fig. 4, D, H, and L). Even after a 3-h treatment with the ligand, a significant amount of the mutant AR still remained in the cytoplasm (Fig. 4, H and L), whereas almost all the signals for the wild-type AR were detected in the nucleus (Fig. 4D). These data indicate that the nuclear translocation and subnuclear localization are impaired in AR-DBD mutants.

To quantitatively analyze the subnuclear foci, 3D images were constructed from the tomographic images collected using the confocal microscope. As shown in Fig. 5, both the C579F and F582Y AR mutants had a much lower number of foci in the nucleus than the wild-type AR. The average number of nuclear foci for the wild-type AR was 300 ± 8, whereas the numbers for F582Y and C579F were 106 ± 18 and 127 ± 23, respectively.

To examine whether the mutant ARs inhibit the nuclear translocation of the wild-type AR, we cotransfected the wild-type AR fused to GFP (AR-WT-GFP) and AR-C579F-CMV (without GFP) and observed the cells under the confocal microscope. Cotransfection of AR-WT-GFP with AR-C579F-CMV showed cytoplasmic dots in addition to fine nuclear foci after treatment with DHT (Fig. 6Ab). Opposite experiments using AR-C579F-GFP and AR-WT-CMV led to similar results, revealing that both nuclear and cytoplasmic dots appeared after incubation with DHT (Fig. 6Ad). To confirm the colocalization of the wild-type and mutant ARs, AR-WT-CFP and AR-C579F-GFP were coexpressed, and each fluorescent signal was collected under the laser confocal microscope. As shown in Fig. 6B, wild-type and mutant ARs were colocalized in both the nuclear and cytoplasmic dots in the presence of 10 nM DHT (Fig. 6B, d–f). The magnitude of the transcriptional activation in the cells transfected with both AR-WT and AR-C579F was less than half that induced by AR-WT (Fig. 6C). In addition to this experiment using 10 nM DHT, we measured the transcriptional activation of the wild-type AR in the presence of 5 nM DHT. The reporter luciferase activity of the wild-type at 5 nM DHT was significantly higher than that by combination of the wild-type and

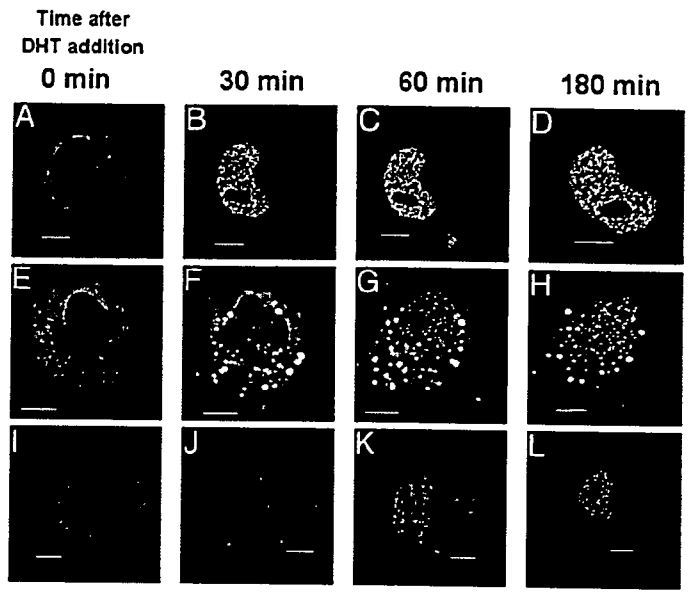

FIG. 4. Time-lapse translocation of wild-type (WT) and mutant ARs after the addition of DHT. COS-7 cells expressing wild-type AR (A–D) or the AR-C579F mutant (E–H and I–L) were treated with 10^{-8} M DHT. Images were collected using a laser confocal microscope before the DHT treatment (A, E, and I) and at 30 (B, F, and J), 60 (C, G, and K), and 180 min (D, H, and L) after the treatment. *Scale bar*, 10 μm.

AR-C579F at 10 nM. Even in a high dose of DHT (100 nM), which can fill all the wild-type LBD, coexpression of AR-C579F inhibited the transcriptional activation mediated by the wild-type AR (Fig. 6C). These results indicated that simple stealing of ligand by AR-C579F is not able to explain the suppression effect of AR-C579F and strongly suggested that AR-C579F is able to form heterodimers with AR-WT in the cells and inhibit the translocation of AR-WT, thereby reducing the transactivation.

As shown in Figs. 4 and 5, the numbers of nuclear foci for the mutant ARs were much lower than that for the wild-type AR. To evaluate whether there are any differences in dynamics between the nuclear foci of the wild-type and mutant ARs, the mobilities of the wild-type and mutant ARs in the nucleus were measured quantitatively by FRAP analysis. After a short period of photobleaching at the maximal power of the laser, continuous images were taken at 1-sec intervals. As shown in Fig. 7A, the recovery of the fluorescence intensity for AR-C579F foci was slower than that for AR-WT. The fluorescence recovery was evaluated by plotting the intensity of the bleached area against time (Fig. 7B). Compared with the wild-type AR, the slope of the fluorescence recovery of AR-C579F was relatively gentle. The $t_{1/2}$ for AR-C579F was 10.5 ± 1.6 sec (n = 12), which was significantly slower than

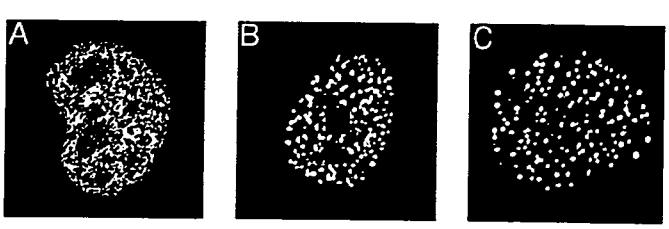

FIG. 5. Three-dimensional image analyses of the intranuclear foci of the wild-type and mutant ARs. COS-7 cells were transfected with 0.5 μg of pAR-GFP (A), pAR-F582Y-GFP (B), or pAR-C579F-GFP (C). Twenty-four hours after the transfection, the cells were treated with DHT and two-dimensional tomographic images collected using the confocal microscope were used to reconstruct 3D images as described in *Subjects and Methods*.

that for the wild-type AR [8.0 ± 1.1 sec (n = 10)]. In another experiment, AR-F582Y also showed reduced mobility, compared with the wild type [$t_{1/2}$ = 8.4 ± 1.1 sec (n = 6)], and the $t_{1/2}$ for AR-F582Y [9.9 ± 1.2 sec (n = 6)] was almost the same as that for AR-C579F [10.2 ± 1.1 sec (n = 6)]. These results indicate that the DBD amino acid substitution in the mutant AR caused decreased mobility of the AR in the nucleus.

As shown in Fig. 3, AR-DBD mutants showed ligand-dependent formation of large cytoplasmic dots. We investigated the localizations of the mutant ARs in the cytoplasm after the ligand treatment. The mutant ARs were not localized in the lysosomes, as shown by an experiment using LysoTracker, a specific marker for lysosomes (data not shown). Next, the mitochondrial localization was examined using MitoTracker, a highly specific probe for mitochondria. Many, but not all, of the cytoplasmic dots of the mutant ARs were located close to mitochondria (Fig. 8A). Because signals for the mutant ARs were not observed in the mitochondria, the mutant ARs do not seem to cross the mitochondrial membrane. To further examine the relationship between the mutant ARs and the mitochondria, immunoelectron microscopy was performed using an anti-GFP antibody. Many gold labels were present around the mitochondria, but none were found inside the mitochondria (Fig. 8Ba). Some clusters were present in the cytoplasm, and these would correspond to the cytoplasmic dots observed by the laser-scanning microscopy (Fig. 8Bb).

Discussion

Using fluorescent proteins and laser-scanning microscopy, we have demonstrated that mutations in the DBD of ARs from AIS patients impair the ligand-dependent nuclear translocation, subnuclear foci formation, and intranuclear mobility of the receptor. In our previous studies, we clearly showed that intranuclear foci formation of AR-GFP was parallel to ligand-dependent transcriptional activation of AR (5, 6). Many studies using GFP-fused steroid hormone receptors have been reported, and linkage of the foci formation of

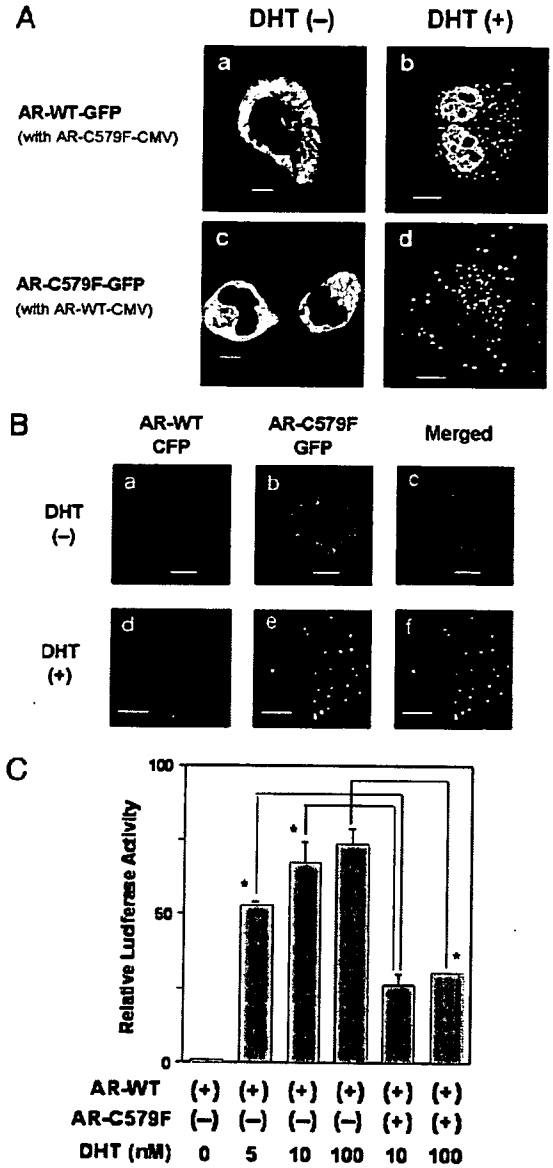

FIG. 6. Coexpression of wild-type and mutant ARs. A, a and b, Equal amounts of AR-WT-GFP and AR-C579F-CMV (without GFP) were cotransfected into COS-7 cells and images were collected before (a) and after (b) the addition of DHT. c and d, COS-7 cells expressing both AR-C579F-GFP and AR-CMV (without GFP) were observed before (c) and after (d) treatment with DHT. If AR WT and mutant proteins have equal chances to form a dimer and formed heterodimer show WT and mutant pattern of signals at an equal rate, the ratio of the intact AR signal *vs.* the abnormal one is expected to be 7:4 (b) and 4:7 (d). Signal patterns of WT and mutant in b and d were consistent with the expected ratios. *Scale bar*, 10 μm. B, Colocalization of wild-type and mutant ARs. AR-WT-CFP and AR-C579F-GFP were coexpressed in COS-7 cells in the absence or presence of DHT. Fluorescent signals were collected using the confocal microscope in the absence (a–c) or presence (d–f) of 10 nM DHT. Signals for AR-WT-CFP (d, *red*) and AR-C579F-GFP (e, *green*) were colocalized (f, merged signals). *Scale bar*, 10 μm. C, AR-C579F inhibited the transactivation mediated by the wild-type AR. COS-7 cells were cotransfected with pGL3-PSA reporter, pRL-CMV, and pAR-CMV with or without pAR-C579F-CMV. After the treatment with or without various concentrations of DHT, the cells were subjected to the luciferase assay. The *bars* show the luciferase activity relative to that of the wild-type AR without DHT. The means ± SD of three independent experiments are shown. *, $P < 0.05$.

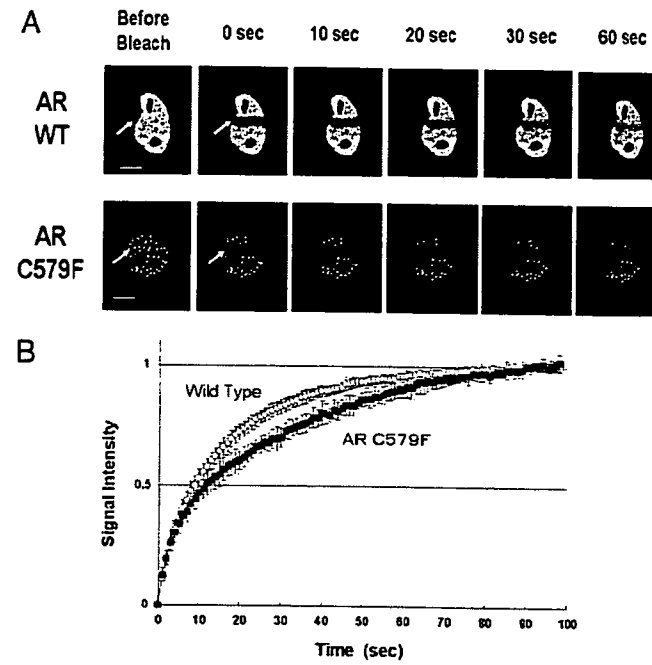

FIG. 7. Comparison of the intranuclear mobilities of the wild-type (WT) and mutant ARs by FRAP analysis. A, FRAP analysis of the intranuclear foci of the wild-type and mutant ARs. COS-7 cells were transfected with a wild-type or mutant AR expression vector. Twenty-four hours after the transfection, the cells were treated with DHT. Five hours after the addition of DHT, a region of interest in the nucleus was photobleached, and images were then taken at the indicated time points using a laser confocal microscope. *Scale bar*, 10 μm. B, Quantification of the fluorescence recovery in the FRAP analysis. The relative fluorescence intensities in the bleached areas of the wild-type and mutant AR foci were plotted. *Open circles*, intensity of the wild-type AR; *closed squares*, intensity of AR-C579F. The means ± SD of 10 cells are shown.

steroid hormone receptors with their transactivation function has been widely accepted (18–20).

There is a significant bias in the distribution of mutations of the AR gene in AIS patients, although the mutations are spread throughout the whole gene (9). Although exon 1 of the AR gene encodes more than half of the AR protein, including the transcription activation domain of the amino terminus, the number of mutations found in this exon is only about 10% of the total number of mutations, and most of the exon 1 mutations are nonsense or frameshift mutations. The mutation hot spots in AIS patients are part of the LBD constituting the pocket for androgen binding. In the DBD, 32 different mutations have been reported and 15 of these were detected in the first zinc finger motif. Most of the mutations in the DBD or LBD are single-base substitutions (3, 9). Some AIS patients do not carry any AR mutations. In such cases, there must be some abnormality in the signal transduction between the AR and the basic transcription machinery, and an impediment in a cofactor interacting with the N-terminal transcription activation domain of the AR has been suggested (14).

The amino acid substitution in the CAIS patient (subject 1) occurred at the cysteine residue contained in the first zinc finger motif of the AR. This AR-C579F mutant would not be able to coordinate the zinc ion, resulting in complete loss of the ligand-dependent DNA-binding ability. In the PAIS patient,

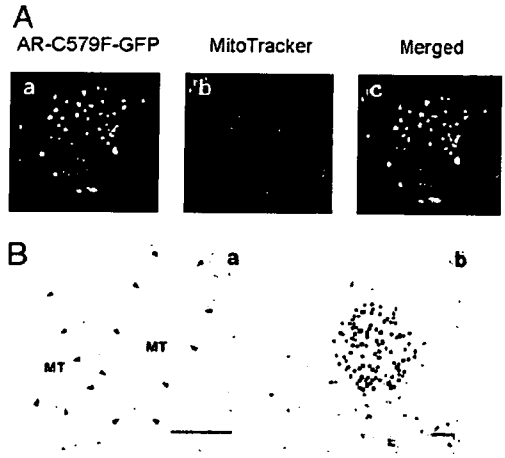

FIG. 8. Mitochondrial localization of cytoplasmic AR-C579F. A, COS-7 cells were transfected with 0.5 μg of AR-C579F-GFP. Twenty-four hours after the transfection, the cells were treated with 10^{-8} M DHT. After a 1-h incubation with DHT, 200 nM MitoTracker-Orange was added to the medium, and the cells were incubated for 30 min. After washing with PBS, the cells were observed under a laser confocal microscope. *Green signals*, AR-C579F-GFP; *red signals*, mitochondria. *Scale bar*, 10 μm. B, Immunoelectron microscopy of the AR-C579F mutant. After treatment with DHT, COS-7 cells expressing AR-C579F-GFP were fixed, embedded, and incubated with an anti-GFP antibody at 4 C overnight, followed by incubation with colloidal gold-conjugated goat antirabbit IgG. Sections were stained and observed with an electron microscope as described in *Subjects and Methods*. a, Low resolution (*bar*, 1 μm); b, high resolution (*bar*, 0.1 μm). MT, Mitochondria. The *arrowheads* show the edges of the mitochondria.

the amino acid substitution (F582Y) occurred next to the P-box and may cause a conformational change of the zinc finger motif. The impaired DNA-binding of these mutant ARs was confirmed by gel mobility shift assays, as we previously reported (11). Before the present imaging analysis, it was anticipated that these mutants would be able to enter the nucleus after ligand treatment but be unable to form foci like the wild-type AR due to the loss of the DNA-binding capacity. However, these mutant ARs initially formed cytoplasmic dots instead of the nuclear foci and nuclear dots subsequently appeared. Because there were no differences among the localizations of the wild-type and mutant ARs in the absence of the ligand, the conformations of the ligand-bound mutant ARs are considered to differ from that of the wild-type AR.

In the present study, ligand-induced formation of cytoplasmic dots of the mutant ARs was observed close to the mitochondria. However, the mutant AR signals were not detected inside the mitochondria by immunoelectron microscopy. Similar findings of an association between cytoplasmic protein aggregates and mitochondria have been observed for other mutant proteins, including the polyQ AR mutants (21–24). The mechanism for such aggregation close to mitochondria has been speculated to be that the ubiquitin-proteasome system tries to degrade a large amount of aggregated proteins and therefore requires an increased amount of ATP around the protein inclusions. The mechanism of localization close to mitochondria for the polyQ AR mutant might also occur for our AR-DBD mutants, although pathophysiology is quite different between our AIS and polyQ diseases. However, further study is necessary for elucidation of abnormal dot formation of our AR mutants.

The C579F mutation in the AR-DBD showed lower mobility than the wild-type AR. FRAP analysis has recently been used to examine the intranuclear dynamics of nuclear receptors (25–27). In the presence of ligands, the mobility of the nuclear receptors was reduced. It has been reported that ligand-induced intranuclear foci formation of steroid hormone receptors is associated with the nuclear matrix in which coactivators are also recruited (28). This nuclear matrix binding induced by ligand treatment is suggested to cause the decreased mobility of the receptors. A glucocorticoid receptor (GR) mutant carrying a deletion of the N-terminal region showed a much lower mobility (26). This mutant was deprived of all the putative phosphorylation sites of the GR. In ATP-deprived cells, GRs are dephosphorylated and tightly bound to the nuclear matrix (29, 30). Therefore, it has been speculated that appropriate reduction of the mobility of steroid hormone receptors, namely nuclear matrix binding with coactivators (6, 31–33), is an essential process for the normal transactivation functions of steroid hormone receptors. Lower or much increased mobility of ligand-bound steroid hormone receptors, as shown for the present AR C579F mutant, may indicate an impaired transactivation process.

The present reanalysis of our mutant ARs unexpectedly revealed two kinds of functional defects, *i.e.* lack of DNA-binding ability reported previously (11) and impairment of translocation from the cytoplasm to the nucleus. The finding that mutations in DNA-binding domain of AR impair nuclear translocation is novel and suggests the existence of an important intramolecular domain for nuclear translocation except for the hinge region. This finding is expected to contribute to the study of translocation mechanism. A mutant AR, K632A/K633A, which has mutations in the hinge region, has an intact DNA-binding domain, but its nuclear translocation is impaired (34). The pattern of the translocation impairment of this AR-K632A/K633A mutant was quite similar to that of our AR mutants, namely the AR-K632A/K633A mutant formed cytoplasmic aggregates (large dots) and its transactivation function examined by a reporter luciferase assay was markedly low (34, 35).

These reported results clearly indicate that impairment of nuclear translocation such as cytoplasmic dot formation can be responsible for the suppression of transactivation function of AR. As is well known, for transactivation function of AR, AR first must be translocated into the nucleus, secondly form a complex with coactivators, and then bind to target genes. Therefore, it would be reasonable that impairment of nuclear translocation in AR-C579F and AR-F582Y is largely responsible for AIS. Abnormal dot formation and decreased mobility of liganded AR-DBD mutants in the nucleus might be due to lack of DNA-binding ability, and thus, a defect in DNA-binding also would be responsible for AIS to some extent. Recent studies have revealed dynamic movement of nuclear receptors during a transactivation process within the nucleus (25, 36, 37). Liganded steroid hormone receptors including AR are transferred to subnuclear compartments (foci) and form a complex with coactivators. These receptor-coactivator complexes are mobilized to the target genes. The

steroid hormone receptors and coactivators show multiphasic on and off for binding to promoter elements of genes. The receptor-coactivator complexes also undergo a rapid exchange between target genes and the compartments. The present AR-DBD mutants are not able to access target genes. This may disturb the dynamic movement (mobility), resulting in prolonged stay at nuclear matrix and abnormal dot formation. This speculation may be supported by the reported observation that the AR-K632A/K633A mutant did not show abnormal intranuclear dot formation, although the authors did not touch on it.

In conclusion, the AR-DBD mutations, C579F and F582Y, found in our AIS patients showed abnormalities in ligand-dependent nuclear translocation, nuclear matrix targeting, and intranuclear mobility of the receptor, which may cause AIS in these patients.

Acknowledgments

We thank Mitoshi Toki for his excellent technical assistance in performing the three-dimensional imaging analyses.

Received January 27, 2005. Accepted August 15, 2005.

Address all correspondence and requests for reprints to: Ryoichi Takayanagi, Department of Geriatric Medicine, Graduate School of Medical Sciences, Kyushu University, 3-1-1 Maidashi, Higashi-ku, Fukuoka 812-8582, Japan. E-mail: takayana@geriat.med.kyushu-u.ac.jp.

This work was supported in part by grants-in-aid for Scientific Research and Exploratory Research and a grant for the 21st Century Center of Excellence Program (Kyushu University) from the Japanese Ministry of Education, Culture, Sports, Science, and Technology.

References

1. **Gobinet J, Poujol N, Sultan Ch** 2002 Molecular action of androgens. Mol Cell Endocrinol 198:15–24
2. **Aranda A, Pascual A** 2001 Nuclear hormone receptors and gene expression. Physiol Rev 81:1269–1304
3. **Brinkmann AO** 2001 Molecular basis of androgen insensitivity. Mol Cell Endocrinol 179:105–109
4. **Roy AK, Tyagi RK, Song CS, Lavrovsky Y, Ahn SC, Oh TS, Chatterjee B** 2001 Androgen receptor: structural domains and functional dynamics after ligand-receptor interaction. Ann NY Acad Sci 949:44–57
5. **Tomura A, Goto K, Morinaga H, Nomura M, Okabe T, Yanase T, Takayanagi R, Nawata H** 2001 The subnuclear three-dimensional image analysis of androgen receptor fused to green fluorescence protein. J Biol Chem 276:28395–28401
6. **Saitoh M, Takayanagi R, Goto K, Fukamizu A, Tomura A, Yanase T, Nawata H** 2002 The presence of both the amino- and carboxyl-terminal domains in the AR is essential for the completion of a transcriptionally active form with coactivators and intranuclear compartmentalization common to the steroid hormone receptors: a three-dimensional imaging study. Mol Endocrinol 16:694–706
7. **Gelmann EP** 2002 Molecular biology of the androgen receptor. J Clin Oncol 20:3001–3015
8. **Balducci R, Ghirri P, Brown TR, Bradford S, Boldrini A, Boscherini B, Sciarra F, Toscano V** 1996 A clinician looks at androgen resistance. Steroids 61:205–211
9. **Gottlieb B, Pinsky L, Beitel LK, Trifiro M** 1999 Androgen insensitivity. Am J Med Genet 89:210–217
10. **McPhaul MJ** 2002 Androgen receptor mutations and androgen insensitivity. Mol Cell Endocrinol 198:61–67
11. **Imasaki K, Okabe T, Murakami H, Tanaka Y, Haji M, Takayanagi R, Nawata H** 1996 Androgen insensitivity syndrome due to new mutations in the DNA-binding domain of the androgen receptor. Mol Cell Endocrinol 120:15–24
12. **Ishizuka M, Kawate H, Takayanagi R, Ohshima H, Tao RH, Hagiwara H** 2005 A zinc finger protein TZF is a novel corepressor of androgen receptor. Biochem Biophys Res Commun 331:1025–1031
13. **Nakao R, Haji M, Yanase T, Ogo A, Takayanagi R, Katsube T, Fukumaki Y, Nawata H** 1992 A single amino acid substitution (Met786–Val) in the steroid-binding domain of human androgen receptor leads to complete androgen insensitivity syndrome. J Clin Endocrinol Metab 74:1152–1157
14. **Adachi M, Takayanagi R, Tomura A, Imasaki K, Kato S, Goto K, Yanase T, Ikuyama S, Nawata H** 2000 Androgen-insensitivity syndrome as a possible coactivator disease. N Engl J Med 343:856–862
15. **Kawate H, Wu Y, Ohnaka K, Nawata H, Takayanagi R** 2005 Tob proteins suppress steroid hormone receptor-mediated transcriptional activation. Mol Cell Endocrinol 230:77–86
16. **Luby-Phelps K, Ning G, Fogerty J, Besharse JC** 2003 Visualization of identified GFP-expressing cells by light and electron microscopy. J Histochem Cytochem 51:271–274
17. **Ham J, Thomson A, Needham M, Webb P, Parker M** 1988 Characterization of response elements for androgens, glucocorticoids and progestins in mouse mammary tumour virus. Nucleic Acids Res 16:5263–5276
18. **Kawata M** 2001 Subcellular steroid/nuclear receptor dynamics. Arch Histol Cytol 64:353–368
19. **DeFranco DB** 2002 Navigating steroid hormone receptors through the nuclear compartment. Mol Endocrinol 16:1449–1455
20. **Hager GL, Nagaich AK, Johnson TA, Walker DA, John S** 2004 Dynamics of nuclear receptor movement and transcription. Biochim Biophys Acta 1677:46–51
21. **Stenoien DL, Cummings CJ, Adams HP, Mancini MG, Patel K, DeMartino GN, Marcelli M, Weigel NL, Mancini MA** 1999 Polyglutamine-expanded androgen receptors from aggregates that sequester heat shock proteins, proteasome components and SRC-1, and are suppressed by the HDJ-2 chaperone. Hum Mol Genet 8:731–741
22. **Waelter S, Boeddrich A, Lurz R, Scherzinger E, Lueder G, Lehrach H, Wanker EE** 2001 Accumulation of mutant huntingtin fragments in aggresome-like inclusion bodies as a result of insufficient protein degradation. Mol Biol Cell 12:1393–1407
23. **Milewski MI, Mickle JE, Forrest JK, Stanton BA, Cutting GR** 2002 Aggregation of misfolded proteins can be a selective process dependent upon peptide composition. J Biol Chem 277:34462–34470
24. **Piccioni F, Pinton P, Simeoni S, Pozzi P, Fascio U, Vismara G, Martini L, Rizzuto R, Poletti A** 2002 Androgen receptor with elongated polyglutamine tract forms aggregates that alter axonal trafficking and mitochondrial distribution in motoneuronal processes. FASEB J 16:1418–1420
25. **Stenoien DL, Patel K, Mancini MG, Dutertre M, Smith CL, O'Malley BW, Mancini MA** 2001 FRAP reveals that mobility of oestrogen receptor-α is ligand- and proteasome-dependent. Nat Cell Biol 3:15–23
26. **Schaaf MJ, Cidlowski JA** 2003 Molecular determinants of glucocorticoid receptor mobility in living cells: the importance of ligand affinity. Mol Cell Biol 23:1922–1934
27. **Maruvada P, Baumann CT, Hager GL, Yen PM** 2003 Dynamic shuttling and intranuclear mobility of nuclear hormone receptors. J Biol Chem 278:12425–12432
28. **Stenoien DL, Mancini MG, Patel K, Allegretto EA, Smith CL, Mancini MA** 2000 Subnuclear trafficking of estrogen receptor-α and steroid receptor coactivator-1. Mol Endocrinol 14:518–534
29. **Hu LM, Bodwell J, Hu JM, Orti E, Munck A** 1994 Glucocorticoid receptors in ATP-depleted cells. Dephosphorylation, loss of hormone binding, HSP90 dissociation, and ATP-dependent cycling. J Biol Chem 269:6571–6577
30. **Tang Y, DeFranco DB** 1996 ATP-dependent release of glucocorticoid receptors from the nuclear matrix. Mol Cell Biol 16:1989–2001
31. **Georget V, Térouanne B, Lumbroso S, Nicolas J-C, Sultan C** 1998 Trafficking of androgen receptor mutants fused to green fluorescent protein: a new investigation of partial androgen insensitivity syndrome. J Clin Endocrinol Metab 83:3597–3603
32. **Nazareth LV, Stenoien DL, Bingman III WE, James AJ, Wu C, Zhang Y, Edwards DP, Mancini M, Marcelli M, Lamb DJ, Weigel NL** 1999 A C619Y mutation in the human androgen receptor causes inactivation and mislocalization of the receptor with concomitant sequestration of SRC-1 (steroid receptor coactivator 1). Mol Endocrinol 13:2065–2075
33. **Karvonen U, Janne OA, Palvimo JJ** 2002 Pure antiandrogens disrupt the recruitment of coactivator GRIP1 to colocalize with androgen receptor in nuclei. FEBS Lett 523:43–47
34. **Thomas M, Dadgar N, Aphale A, Harrell JM, Kunkel R, Pratt WB, Lieberman AP** 2004 Androgen receptor acetylation site mutations cause trafficking defects, misfolding, and aggregation similar to expanded glutamine tracts. J Biol Chem 279:8389–8395
35. **Fu M, Wang C, Reutens AT, Wang J, Angeletti RH, Siconolfi-Baez L, Ogryzko V, Avantaggiati ML, Pestell RG** 2000 p300 and p300/cAMP-response element-binding protein-associated factor acetylate the androgen receptor at sites governing hormone-dependent transactivation. J Biol Chem 275:20853–20860
36. **Métivier R, Penot G, Hübner MR, Reid G, Brand H, Koš M, Gannon F** 2003 Estrogen receptor-α directs ordered, cyclical, and combinational recruitment of cofactors on a natural target promoter. Cell 115:751–763
37. **McNally JG, Muller WG, Walker D, Wolford R, Hager GL** 2000 The glucocorticoid receptor: rapid exchange with regulatory sites in living cells. Science 287:1262–1265

THE JOURNAL OF BIOLOGICAL CHEMISTRY VOL. 280, NO. 43, pp. 36355–36363, October 28, 2005

Modulation of Androgen Receptor Transactivation by FoxH1

*A NEWLY IDENTIFIED ANDROGEN RECEPTOR COREPRESSOR**

Received for publication, June 6, 2005, and in revised form, August 11, 2005 Published, JBC Papers in Press, August 23, 2005, DOI 10.1074/jbc.M506147200

Guangchun Chen[‡§1], Masatoshi Nomura[‡2], Hidetaka Morinaga[‡], Eri Matsubara[‡], Taijiro Okabe[‡], Kiminobu Goto[‡], Toshihiko Yanase[‡], Hong Zheng[¶], Jian Lu[§], and Hajime Nawata[‡]

From the [‡]Department of Medicine and Bioregulatory Science, Graduate School of Medical Science, Kyushu University, Maidashi 3-1-1, Higashi-ku, Fukuoka 812-8582, Japan and [§]Department of Pathophysiology and [¶]Laboratory Center of Pharmacology, Second Military Medical University, 800, Xiang Yin Road, Shanghai 200433, China

Androgen signaling plays key roles in the development and progression of prostate cancer, and numerous ongoing studies focus on the regulation of androgen receptor (AR) transactivity to develop novel therapies for the treatment of androgen-independent prostate cancer. FoxH1, a member of the Forkhead-box (FOX) gene family of transcription factors, takes part in mediating transforming growth factor-β/activin signaling through its interaction with the Smad2·Smad4 complex. Using a series of experiments, we found that FoxH1 repressed both ligand-dependent and -independent transactivation of the AR on androgen-induced promoters. This action of FoxH1 was independent of its transactivation capacity and activin A but relieved by Smad2·Smad4. In addition, the repression of the AR by FoxH1 did not require deacetylase activity. A protein-protein interaction was identified between the AR and FoxH1 independently of dihydrotestosterone. Furthermore, a confocal microscopic analysis of LNCaP cells revealed that the interaction between the AR and FoxH1 occurred in the nucleus and that FoxH1 specifically blocked the foci formation of dihydrotestosterone-activated AR, which has been shown to be correlated with the AR transactivation potential. Taken together, our results indicate that FoxH1 functions as a new corepressor of the AR. Our observations not only strengthen the role of FoxH1 in AR-mediated transactivation but also suggest that therapeutic interventions based on AR-coregulator interactions could be designed to block both androgen-dependent and -independent growth of prostate cancer.

Prostate cancer is a significant cause of morbidity and mortality worldwide. Androgens play major roles in promoting the development and progression of prostate cancer (1–3), and therefore, androgen ablation and blockade of androgen actions through the androgen receptor (AR)[3] have been the cornerstones of treatments for advanced prostate cancer. Despite these regimens, prostate cancer invariably progresses to a fatal, androgen-refractory state (4, 5). However, although such relapsed tumors are androgen-independent, they are still dependent on the AR for their growth and survival (4, 6–8). Therefore, identification of the precise mechanisms underlying the regulation of AR function is of critical importance for the design and development of novel therapies and pharmaceutical targets for treating prostate cancers.

The AR shares a characteristic structure with other members of the steroid hormone receptor family (comprised of receptors for estrogens (ERs), progesterone (PR), glucocorticoids (GR), and mineralocorticoids), namely a variable NH_2-terminal transactivation domain (NTD) possessing an activation function 1 (AF-1) domain, a highly conserved zinc finger-type DNA binding domain (DBD), and a ligand binding domain (LBD) that usually contains a second activation domain (AF-2) (9, 10). AF-1 functions in a ligand-independent manner, whereas the activity of AF-2 requires cognate ligand binding (9, 11, 12). Upon activation by ligands, the AR translocates to the nucleus, where it binds to androgen response elements and regulates the transcription of target genes. Moreover, it has become clear that the transactivity of nuclear receptors, including the AR, is regulated by coregulator proteins that enhance (coactivators) or reduce (corepressors) the target gene transcription by various mechanisms (10, 13, 14). Although most of the AR coregulators identified to date have been coactivators, it is conceivable that AR corepressors are also required for precise and efficient regulation of the AR activity in cells (13, 15). Therefore, further characterization of AR corepressors may provide insights into the signaling events that occur within prostate cancer and pave the way to the development of individualized therapies.

Activins, which are members of the TGF-β superfamily, are composed of two β subunits, βA and βB, which form activin A (βAβA), activin B (βBβB), and activin AB (βAβB) (16). In addition to their stimulatory effects on pituitary follicle-stimulating hormone synthesis, activins have also been implicated in the control of many other cellular processes, including growth and tumorigenesis (17, 18). The presence of activin A and its receptors in the prostate (19–22) and the ability of activin A to inhibit prostate cancer cells grown in culture (23–26) suggest an important role for activin A in the regulation of prostatic growth. Moreover, activin A has been shown to induce the expression of prostate-specific antigen (PSA), prostatic acid phosphatase, and the AR (26), genes that are also induced by androgen. Although the molecular mechanism through which activin A regulates gene expression and growth in the prostate has not yet been fully elucidated, cross-talk between activin A and androgen-mediated signaling pathways may play critical roles in these processes (27).

Smads are a family of proteins that function as effectors of the TGF-β/activin-signaling pathway. Ligand addition induces the phosphorylation of specific receptor-regulated Smads (R-Smads), which then oligomerize with the common mediator Smad4 and move into the nucleus. Once there, the R-Smad·Smad4 complex interacts with a vari-

* This work was supported in part by a grant-in-aid for Scientific Research from the Ministry of Education, Science, Sports and Culture, Japan. The costs of publication of this article were defrayed in part by the payment of page charges. This article must therefore be hereby marked "*advertisement*" in accordance with 18 U.S.C. Section 1734 solely to indicate this fact.

[1] Supported in part by a Sasakawa Medical Grant from the Japan-China Medical Association.

[2] To whom correspondence should be addressed. Tel.: 81-92-642-5280; Fax: 81-92-642-5297; E-mail: nomura@med.kyushu-u.ac.jp.

[3] The abbreviations used are: AR, androgen receptor; ER, estrogen receptor; PR, progesterone receptor; GR, glucocorticoid receptor; NTD, NH_2-terminal transactivation domain; AF-1, activation function 1; DBD, DNA binding domain; LBD, ligand binding domain; AF-2, activation domain 2; PSA, prostate-specific antigen; TGIF, 5′TG3′ interacting factor; GFP, green fluorescent protein; MMTV, mouse mammary tumor virus; LUC, luciferase; DHT, dihydrotestosterone; TSA, trichostatin A; TGF, transforming growth factor; CBP, cAMP-response element-binding protein (CREB)-binding protein; RT, reverse transcription.

ety of transcription factors and coregulators and becomes targeted to a diverse array of gene promoters (28, 29). Interestingly, some coregulators of Smads, such as AP-1 (30), CBP/P300 (31, 32), and TGIF (33), can also regulate AR-mediated transactivation (34–37). FoxH1 (also known as FAST-1), a member of the Forkhead-box (FOX) gene family of transcription factors, plays an important role in mediating TGF-β/activin signals through its interaction with the Smad2·Smad4 complex (38–40). We hypothesized that FoxH1 may also function as a coregulator to regulate the AR transactivation potential and, therefore, be involved in the cross-talk between activin A and androgen-mediated signaling. In the present study we found that FoxH1 could repress ligand-dependent and -independent transactivation of the AR on androgen-induced promoters. However, the repression of the AR by FoxH1 was not alleviated by activin A, indicating that FoxH1 was dispensable for the stimulatory effect of activin A on PSA expression (26, 27, 41). Nonetheless, our results demonstrate that FoxH1 is a new corepressor of the AR.

EXPERIMENTAL PROCEDURES

Plasmids—pCMVhAR, pCMXhGR, pcDNA3-ANT-1, pcDNA3-Smad2, pcDNA3-Smad4, pAR-GFP, and pCBP-GFP as well as the reporter plasmid pMMTV-LUC (containing the luciferase gene driven by the mouse mammary tumor virus (MMTV) long terminal repeat harboring hormone response elements for AR, GR, and PR) were described previously (42–47). The human FoxH1 expression vectors pCMVFoxH1 and pCMVFoxH1$_{H83R}$ were kindly provided by Dr. Bert Vogelstein (Howard Hughes Medical Institute, Johns Hopkins Oncology Center, Baltimore, MD) (39). The human ER expression vectors pSG5-ERα and pSG5-ERβ as well as a reporter plasmid for ER (pERE2-tk109-LUC) were kind gifts from Dr. Shigeaki Kato (University of Tokyo, Tokyo, Japan). The reporter plasmid pPSA-LUC, containing the luciferase gene under the control of a 6.1-kilobase promoter fragment of the human PSA gene, was kindly provided by Dr. Jer-Tsong Hsieh (University of Texas Southwestern Medical Center, Dallas, TX). The human PR expression vectors pSG5-PRA and pSG5-PRB were kind gifts from Dr. Pierre Chambon (INSERM, Illkirch, France). pRL-SV40, pG5-LUC, pBIND, and pACT expression vectors were obtained from Promega (Madison, WI).

AR and FoxH1 expression vectors for mammalian two-hybrid assays were subcloned into the pBIND and pACT expression vectors, respectively. pFoxH1-Myc and pFoxH1$_{H83R}$-Myc were constructed by subcloning the FoxH1 and FoxH1$_{H83R}$ cDNAs into pcDNA3.1/Myc-His, respectively. pFoxH1-GFP was constructed by inserting the FoxH1 cDNA into pEGFP-N1 (BD Biosciences Clontech, Palo Alto, CA). The validity of the structure of each construct was confirmed by DNA sequencing and Western blot analysis of transfected COS-7 cells.

RNA Preparation and RT-PCR—Total RNA was extracted using ISOGENE (Wako, Osaka, Japan) according to the manufacturer's instructions. The concentration and purity of the RNA were determined spectrophotometrically. Next, 5 μg of total RNA was reverse-transcribed into first-strand cDNA using a SuperScript III kit (Invitrogen) in a final volume of 20 μl. To analyze the expression of FoxH1 in prostate cancer cell lines, a sensitive RT-PCR was performed using previously described primers (39). The PCR was carried out in a 50-μl reaction mixture containing 2.5 mM $MgCl_2$, 0.3 mM dNTP, and 2.5 units of *Taq* DNA polymerase (Promega) under the following conditions: 35 cycles of denaturation at 94 °C for 30 s, annealing at 58 °C for 30 s, and extension at 72 °C for 1 min. Aliquots of the PCR products were electrophoresed in 2% agarose gels containing 0.5 mg/ml ethidium bromide and then photographed under UV light using a positive/negative instant film (Polaroid 665; Nippon-Polaroid, Tokyo, Japan). The authenticity of each PCR product was confirmed by sequencing.

Transactivation Assays—The human prostate cancer cell lines LNCaP and PC-3 were maintained in RPMI 1640 medium (Sigma) supplemented with 10% fetal bovine serum (Sera Laboratories Ltd., Sussex, UK). COS-7 monkey kidney cells and ALVA41 human prostate cancer cells were maintained in Dulbecco's modified Eagle's medium supplemented with 10% fetal bovine serum. The cells were cotransfected with the indicated expression vectors in 24-well plates using an Effectene transfection kit (Qiagen K. K., Tokyo, Japan) according to the manufacturer's protocol. The cells were then incubated in RPMI 1640 or Dulbecco's modified Eagle's medium containing 0.5% dextran-coated charcoal-stripped fetal bovine serum and vehicle (0.1% ethanol) or ligands as indicated. After 24 h, the firefly and *Renilla* luciferase activities were assayed using the Dual-Luciferase® Reporter assay system (Promega) according to the manufacturer's protocol in a Minilumat LB9507 (Berthold Technologies, Bad Wildbad, Germany). The results were normalized for the internal *Renilla* control and presented as the relative luciferase activity. All transfection experiments were carried out in triplicate wells and repeated at least three times using two sets of plasmids prepared separately. Data were calculated as the mean ± S.D.

Stable Transfection of LNCaP Cells with pFoxH1-Myc, Semiquantitative RT-PCR, and Western Blotting—LNCaP cells were cultured in six-well plates and then transfected with pFoxH1-Myc using an Effectene transfection kit. After 4 weeks of culturing and selection with 400 μg/ml of Geneticin (Invitrogen), 6 colonies were harvested. After limited dilution, 2 independent FoxH1-Myc-expressing clones (designated LNCaP/FoxH1-1 and LNCaP/FoxH1-2) were identified by Western blotting with an anti-Myc antibody (1:1000; sc-40; Santa Cruz Biotechnology, Inc.) and further maintained as stable cell lines in RPMI 1640 supplemented with 200 μg/ml Geneticin. Cells stably transfected with the empty vector (LNCaP/Vector) served as a control.

The effect of stably expressing FoxH1 on the endogenous PSA level in the absence or presence of 100 nM dihydrotestosterone (DHT) was investigated by semiquantitative RT-PCR and Western blotting, respectively. For semiquantitative RT-PCR, total RNA was extracted and reverse-transcribed as described above. Preliminary experiments were conducted to ensure linearity for the semiquantitative procedures. Hot-start PCR was performed by heat-activating AmpliTaq Gold DNA polymerase (PerkinElmer Life Sciences) at 95 °C for 10 min. Optimized cycling condition was 30 cycles (for PSA) or 26 cycles (for glyceraldehyde-3-phosphate dehydrogenase) of 1 min at 94 °C, 1 min at 56 °C, and 1 min at 72 °C. The primer sequences specific for PSA and glyceraldehyde-3-phosphate dehydrogenase were described previously (48, 49). For Western blotting, the cells were harvested, and the protein concentration of each sample was measured using a BCA protein assay kit (Pierce). Aliquots containing 20 μg of protein were separated in 10% SDS-PAGE gels and transferred onto nitrocellulose membranes. Next, the membranes were probed with the anti-human PSA antibody A67-B/E3 (1:200; sc-7316; Santa Cruz Biotechnology Inc.) or an anti-β-actin antibody (1:500; AC-74; Sigma). Bands were visualized using an alkaline phosphatase system.

Microscopy and Imaging Analyses—Microscopy and imaging analyses were performed essentially as described previously (44–46). The cells were imaged for green fluorescence by excitation with the 488-nm line from an argon laser, and the emission was viewed through a 496–505-nm band pass filter.

Immunoprecipitation and Western Blotting—COS-7 cells were cotransfected with 2 μg of pFoxH1-Myc or pFoxH1$_{H83R}$-Myc together